

# Structures and Partial Stereochemical Assignments for Prymnesin-1 and Prymnesin-2: Potent Hemolytic and Ichthyotoxic Glycosides Isolated from the Red Tide Alga *Prymnesium parvum*

Tomoji Igarashi<sup>\*,†</sup> Masayuki Satake, and Takeshi Yasumoto<sup>\*,†</sup>

Contribution from the Department of Applied Biochemistry, Graduate School of Agricultural Science, Tohoku University, Sendai, Japan

Received May 25, 1999

**Abstract:** Two glycosidic toxins, prymnesin-1 (PRM1) and prymnesin-2 (PRM2) have been isolated from cultured cells of the red tide phytoflagellate *Prymnesium parvum*, and the gross structure of PRM2 C<sub>96</sub>H<sub>136</sub>Cl<sub>3</sub>NO<sub>35</sub> has been reported in a previous contribution. The molecule possesses unique structural features: a C<sub>90</sub> unbranched carbon chain except for a single methyl, five contiguous ether rings (6/6/6/7/6), four distinct 1,6-dioxadecalin units, conjugated double and triple bonds, chlorine and nitrogen atoms, and an uncommon L-xylose. Potent ichthyotoxic and hemolytic properties of the two toxins were also demonstrated. However, the stereochemistry of PRM2 and the structure of PRM1 remained unknown. In the present paper the relative stereochemistry of the polycyclic ether moiety of PRM2 and the structure of PRM1 C<sub>107</sub>H<sub>154</sub>Cl<sub>3</sub>NO<sub>44</sub> are reported. Structural elucidation was carried out by extensive analysis of NMR data. Difficulties arising from the poor solubility of the toxins in NMR solvents were overcome by preparing *N*-acetyl, peracetyl, perhydro, and dehydrochlorinated derivatives of the toxins. These derivatives were also effective in improving the precision of signal assignments. <sup>13</sup>C NMR measurements were facilitated by a <sup>13</sup>C-enriched *N*-acetate from cultures of the flagellate in the presence of Na<sup>13</sup>CO<sub>3</sub>. Comparison of the NMR data between *N*-acetylprymnesin-1 and *N*-acetylprymnesin-2 and chiral GC analysis of the glycosidic residues indicated that PRM1 possessed α-D-ribofuranosyl, α-L-arabinopyranosyl, and β-D-galactofuranosyl residues at C77, C78, and C82 positions, respectively, on the same aglycone structure as PRM2. In the polycyclic parts (C20–C74) of both toxins, all ring fusions were *trans* and all rings took a chair conformation. The stereochemistry at C14 and C76–C85 remains unknown.

## Introduction

Massive fish kills due to algal blooms (red tides) are a global phenomenon and are suspected to have increased in both frequency and geographical distribution as a result of eutrophication of coastal waters. In addition to the immense economic damage to fish farming industries, these blooms may have devastating effects on coastal ecology by killing virtually all benthic animals and algae. *Prymnesium parvum*<sup>1</sup> is one of the causative red tide organisms for such natural catastrophes, which occur worldwide<sup>2</sup> in low-salinity water as exemplified by the massive fish kills at carp ponds in Israel during the 1940s–1960s<sup>3</sup> and on Scandinavian salmon farms during the 1980s–1990s.<sup>4</sup> Prymnesin, the potent hemolytic and ichthyotoxic agent produced by *P. parvum*, has been shown to be implicated in these cases.<sup>5</sup> However, the chemical nature of the toxins

remained unknown until recently,<sup>6</sup> due to the extreme difficulty of isolation coupled with the complexity of the molecules. In a previous communication,<sup>7</sup> we reported the planar structure of one of the two major toxins, prymnesin-2 (C<sub>96</sub>H<sub>136</sub>Cl<sub>3</sub>NO<sub>35</sub>), which consists of a polycyclic ether moiety and polyhydroxy and polyene side chains. However, the structure of prymnesin-1 and the stereochemistry of both prymnesins remained unknown. In the present paper, we report the structural elucidation of prymnesin-1 (PRM1, **1**) and prymnesin-2 (PRM2, **2**) including partial stereochemical assignments (Figure 1).

## Results and Discussion

**Biological and Chemical Properties of Prymnesins.** PRM1 and PRM2 used in this study were purified from cultured cells of *P. parvum* as described in the Experimental Section. The details of the biological properties of the prymnesins are reported separately;<sup>8</sup> briefly, the biological activities of PRM1 and PRM2 are almost the same. Both toxins possess extremely potent hemolytic activity (around 3 nM), which is about 50000-fold

<sup>†</sup> Current address: Japan Food Research Laboratories, Tama Laboratory 6-11-10, Nagayama, Tama-shi, Tokyo 206-0025, Japan.

(1) *Prymnesium parvum* was first described by Carter, N. *Arch. Protistenk.* **1937**, *90*, 40–43. It belongs to the haptophytes and differs markedly from the dinophytes that are often involved in seafood poisoning by producing the brevetoxins, ciguatoxins, and saxitoxins, etc.

(2) Otterström, C. V.; Steemann-Nielsen, E. *Rep. Dan. Biol. Sta.* **1939**, *44*, 5–24.

(3) Shilo, M.; Aschner, M. *J. Gen. Microbiol.* **1953**, *8*, 333–343.

(4) (a) Eikrem, W.; Throndsen, J. In *Toxic Phytoplankton Blooms in the Sea*; Smayda, T. J., Shimizu, Y. Eds.; Elsevier: Amsterdam, 1993; pp 687–692. (b) Lindholm, T.; Virtanen, T. *Environ. Toxic. Water Qual.* **1992**, *7*, 165–170.

(5) Yariv, J.; Hestrin, S. *J. Gen. Microbiol.* **1961**, *24*, 165–175.

(6) Yariv and Hestrin alleged the toxic principle to be a saponin,<sup>5</sup> Paster, a glycolipid,<sup>6a</sup> and Ulitzur and Shilo, a proteolipid.<sup>6b</sup> Attribution of the diverse biological activities to a single molecule was questioned in a review by Parnas:<sup>6c</sup> (a) Paster, *Z. Rev. Int. Oceanogr. Med.* **1968**, *10*, 249–258. (b) Ulitzur, S.; Shilo, M. *Biochim. Biophys. Acta* **1970**, *201*, 350–363. (c) Parnas, I. *J. Zool.* **1963**, *12*, 15–23.

(7) Igarashi, T.; Satake, M.; Yasumoto, T. *J. Am. Chem. Soc.* **1996**, *118*, 479–480.

(8) Igarashi, T.; Aritake, S.; Yasumoto, T. *Nat. Toxins* **1998**, *6*, 35–41.



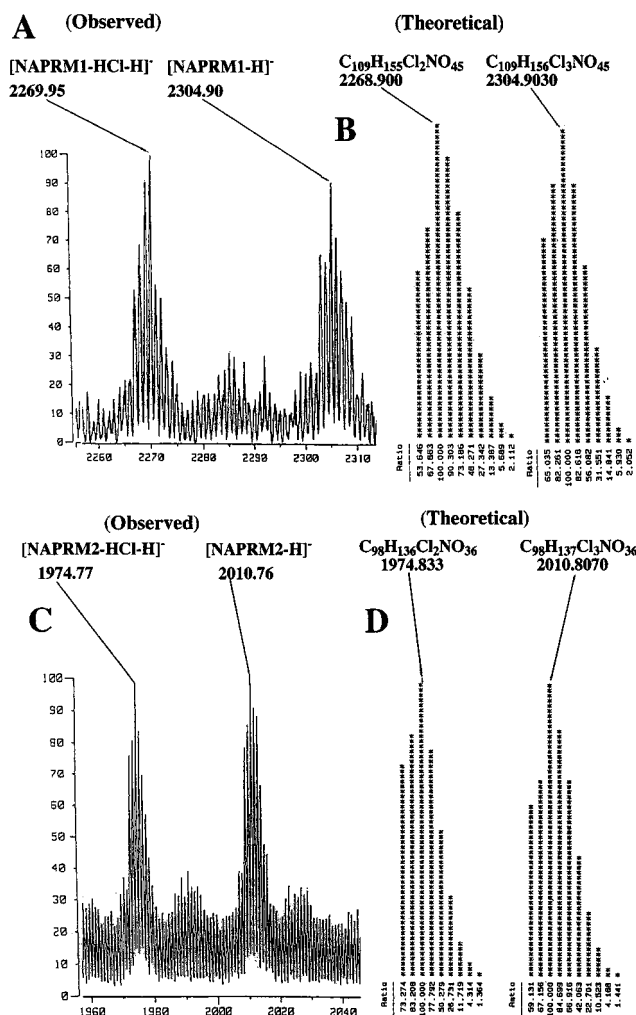


**Figure 2.** Negative FAB MS spectra of NAPRM1 (A) and NAPRM2 (C), and the theoretical ion distribution data for dechlorodehydro-*N*-acetylprymnesin-1  $C_{109}H_{155}Cl_2NO_{45}$  and *N*-acetylprymnesin-1  $C_{109}H_{156}Cl_3NO_{45}$  (B), and for dechlorodehydro-*N*-acetylprymnesin-2  $C_{98}H_{136}Cl_2NO_{36}$ , and *N*-acetylprymnesin-2  $C_{98}H_{137}Cl_3NO_{36}$  (D).

three obstacles. First and most importantly, their solubilities were extremely low in NMR solvents, in single use or, in mixtures; e.g., the maximum concentration in the optimum solvent  $CD_3OD/C_5D_5N$  (1:1) was less than 1 mM, which resulted in low signal-to-noise ratios even in the proton NMR spectra. Second, since they possessed two sets of contiguous acetylenic bonds, the long-range couplings through these bonds were difficult to interpret. Third, three chlorine atoms in the molecules made it difficult to distinguish the protons on chlorinated carbons from those on oxygenated carbons. To overcome these obstacles, we first targeted PRM2, since it appeared to be smaller and less complicated than PRM1. PRM2 was derivatized to its *N*-acetate, peracetate, 1-dechloro-perhydroPRM2, 85-dechloro-86-dehydroPRM2, and *N*-acetyl-85-dechloro-86-dehydro PRM2 in order to improve the solubility and/or to achieve better separation of some signals. The solubilities of the prymnesins were improved by *N*-acetylation, which led to the detection of more than 95% of the proton cross-peaks in the  $^1H-^1H$  COSY spectra of both prymnesins. In the spectra of peracetylprymnesin-2 (PAPRM2), the heavily overlapped proton signals (2.8–4.5 ppm) on oxygenated carbons in PRM2 were partly solved by the downfield shifts of the acetoxy methine protons. Thus, locating an amino group and hydroxyl groups, respectively, was accomplished by the NMR data of NAPRM2 and PAPRM2.

1-Dechloro-perhydroprymnesin-2 (HPRM2) was used to determine the number of unsaturated bonds in the molecule. 85-Dechloro-86-dehydroprymnesin-2 (PRM2-HCl) and its *N*-acetate (NAPRM2-HCl) were used to verify the presence of conjugated triple bonds in the termini and the chlorine atom at C85. The data explained the occurrence of dehydrochlorinated ions  $[M - HCl - H]^-$  in the negative FABMS of NAPRM1 and NAPRM2. As another approach to overcome the problems of low solubilities, especially in measurements of  $^{13}C-^1H$  correlation NMR spectra,  $^{13}C$ -enrichment of the two toxins was carried out by culturing *P. parvum* in the presence of  $Na_2^{13}CO_3$ . The incorporation ratio was estimated to be about 5:1 by comparison of the  $^{13}C$  signal intensities between the C91-methyl and the acetyl-methyl group introduced by *N*-acetylation on the broad-band proton-decoupled spectrum of  $^{13}C$ -enriched NAPRM2. In addition, four solvents were used for NMR measurements to improve signal separation by solvent effect and to increase the solubility of the derivatives.  $CD_3OD/CD_3COOD$  (19:1) was used for PRM1 and PRM2; dioxane- $d_8/D_2O/CD_3COOD$  (10:10:1) for NAPRM2;  $CD_3OD/C_5D_5N$  (1:1) for NAPRM1, NAPRM2, PAPRM2, and HPRM2; and  $CD_3CN/D_2O$  (9:1) for PAPRM2. The structure of PRM1 was chiefly elucidated by comparing the NMR data of NAPRM1 to those of NAPRM2.

**Overview of the Molecules.** On the basis of the  $^1H$ -1D spectra of NAPRM1 and NAPRM2 shown in Figure 3, they were found to have similar structural features. One acetyl methyl signal at about 1.9 ppm supported the presence of at least one amino group in both molecules, as assumed by the MS data. Abundance of signals observed between 2.8 and 4.5 ppm suggested the presence of a great number of hydroxyl groups or other oxygens analogous with maitotoxin.<sup>11</sup> Unlike maitotoxin, however, there was no singlet methyl signal and this implied the absence of any quaternary ether carbon substituted with an angular methyl group on an ether ring.

**Planar Structure of Prymnesin-2.** In our previous contribution,<sup>7</sup> we briefly described the elucidation of the planar structure of PRM2. Here we describe the process in more detail, since the planar structure of PRM2 is the basis for elucidating not only the planar structure of PRM1 but also its stereochemistry. As described above, the NMR data of the  $^{13}C$ -enriched specimen of NAPRM2 (1.5 mg) were chiefly used for this structural elucidation.

Extensive analyses of  $^1H-^1H$  COSY and TOCSY spectra of NAPRM2 measured at 500 MHz in  $CD_3OD/C_5D_5N$  (1:1), and DQF COSY and HOHAHA spectra of NAPRM2-HCl measured at 600 MHz in the same solvent, permitted us to deduce the partial structures encompassing H1–H2, H5–H6, H9–H10, H12–H13, H16–H17, H19–H20, H22–H23, H26–H27, H29–H30, H33–H34, H37–H38, H41–H42, H45–H46, H49–H50, H53–H54, H57–H58, H61–H62, H65–H66, H69–H70, H73–H74, H77–H78, H81–H82, H85–H86, H89–H90, H93–H94, H97–H98, H101–H102, H105–H106, H109–H110, H113–H114, H117–H118, H121–H122, H125–H126, H129–H130, H133–H134, H137–H138, H141–H142, H145–H146, H149–H150, H153–H154, H157–H158, H161–H162, H165–H166, H169–H170, H173–H174, H177–H178, H181–H182, H185–H186, H189–H190, H193–H194, H197–H198, H201–H202, H205–H206, H209–H210, H213–H214, H217–H218, H221–H222, H225–H226, H229–H230, H233–H234, H237–H238, H241–H242, H245–H246, H249–H250, H253–H254, H257–H258, H261–H262, H265–H266, H269–H270, H273–H274, H277–H278, H281–H282, H285–H286, H289–H290, H293–H294, H297–H298, H301–H302, H305–H306, H309–H310, H313–H314, H317–H318, H321–H322, H325–H326, H329–H330, H333–H334, H337–H338, H341–H342, H345–H346, H349–H350, H353–H354, H357–H358, H361–H362, H365–H366, H369–H370, H373–H374, H377–H378, H381–H382, H385–H386, H389–H390, H393–H394, H397–H398, H401–H402, H405–H406, H409–H410, H413–H414, H417–H418, H421–H422, H425–H426, H429–H430, H433–H434, H437–H438, H441–H442, H445–H446, H449–H450, H453–H454, H457–H458, H461–H462, H465–H466, H469–H470, H473–H474, H477–H478, H481–H482, H485–H486, H489–H490, H493–H494, H497–H498, H501–H502, H505–H506, H509–H510, H513–H514, H517–H518, H521–H522, H525–H526, H529–H530, H533–H534, H537–H538, H541–H542, H545–H546, H549–H550, H553–H554, H557–H558, H561–H562, H565–H566, H569–H570, H573–H574, H577–H578, H581–H582, H585–H586, H589–H590, H593–H594, H597–H598, H601–H602, H605–H606, H609–H610, H613–H614, H617–H618, H621–H622, H625–H626, H629–H630, H633–H634, H637–H638, H641–H642, H645–H646, H649–H650, H653–H654, H657–H658, H661–H662, H665–H666, H669–H670, H673–H674, H677–H678, H681–H682, H685–H686, H689–H690, H693–H694, H697–H698, H701–H702, H705–H706, H709–H710, H713–H714, H717–H718, H721–H722, H725–H726, H729–H730, H733–H734, H737–H738, H741–H742, H745–H746, H749–H750, H753–H754, H757–H758, H761–H762, H765–H766, H769–H770, H773–H774, H777–H778, H781–H782, H785–H786, H789–H790, H793–H794, H797–H798, H801–H802, H805–H806, H809–H810, H813–H814, H817–H818, H821–H822, H825–H826, H829–H830, H833–H834, H837–H838, H841–H842, H845–H846, H849–H850, H853–H854, H857–H858, H861–H862, H865–H866, H869–H870, H873–H874, H877–H878, H881–H882, H885–H886, H889–H890, H893–H894, H897–H898, H901–H902, H905–H906, H909–H910, H913–H914, H917–H918, H921–H922, H925–H926, H929–H930, H933–H934, H937–H938, H941–H942, H945–H946, H949–H950, H953–H954, H957–H958, H961–H962, H965–H966, H969–H970, H973–H974, H977–H978, H981–H982, H985–H986, H989–H990, H993–H994, H997–H998, H1001–H1002, H1005–H1006, H1009–H1010, H1013–H1014, H1017–H1018, H1021–H1022, H1025–H1026, H1029–H1030, H1033–H1034, H1037–H1038, H1041–H1042, H1045–H1046, H1049–H1050, H1053–H1054, H1057–H1058, H1061–H1062, H1065–H1066, H1069–H1070, H1073–H1074, H1077–H1078, H1081–H1082, H1085–H1086, H1089–H1090, H1093–H1094, H1097–H1098, H1101–H1102, H1105–H1106, H1109–H1110, H1113–H1114, H1117–H1118, H1121–H1122, H1125–H1126, H1129–H1130, H1133–H1134, H1137–H1138, H1141–H1142, H1145–H1146, H1149–H1150, H1153–H1154, H1157–H1158, H1161–H1162, H1165–H1166, H1169–H1170, H1173–H1174, H1177–H1178, H1181–H1182, H1185–H1186, H1189–H1190, H1193–H1194, H1197–H1198, H1201–H1202, H1205–H1206, H1209–H1210, H1213–H1214, H1217–H1218, H1221–H1222, H1225–H1226, H1229–H1230, H1233–H1234, H1237–H1238, H1241–H1242, H1245–H1246, H1249–H1250, H1253–H1254, H1257–H1258, H1261–H1262, H1265–H1266, H1269–H1270, H1273–H1274, H1277–H1278, H1281–H1282, H1285–H1286, H1289–H1290, H1293–H1294, H1297–H1298, H1301–H1302, H1305–H1306, H1309–H1310, H1313–H1314, H1317–H1318, H1321–H1322, H1325–H1326, H1329–H1330, H1333–H1334, H1337–H1338, H1341–H1342, H1345–H1346, H1349–H1350, H1353–H1354, H1357–H1358, H1361–H1362, H1365–H1366, H1369–H1370, H1373–H1374, H1377–H1378, H1381–H1382, H1385–H1386, H1389–H1390, H1393–H1394, H1397–H1398, H1401–H1402, H1405–H1406, H1409–H1410, H1413–H1414, H1417–H1418, H1421–H1422, H1425–H1426, H1429–H1430, H1433–H1434, H1437–H1438, H1441–H1442, H1445–H1446, H1449–H1450, H1453–H1454, H1457–H1458, H1461–H1462, H1465–H1466, H1469–H1470, H1473–H1474, H1477–H1478, H1481–H1482, H1485–H1486, H1489–H1490, H1493–H1494, H1497–H1498, H1501–H1502, H1505–H1506, H1509–H1510, H1513–H1514, H1517–H1518, H1521–H1522, H1525–H1526, H1529–H1530, H1533–H1534, H1537–H1538, H1541–H1542, H1545–H1546, H1549–H1550, H1553–H1554, H1557–H1558, H1561–H1562, H1565–H1566, H1569–H1570, H1573–H1574, H1577–H1578, H1581–H1582, H1585–H1586, H1589–H1590, H1593–H1594, H1597–H1598, H1601–H1602, H1605–H1606, H1609–H1610, H1613–H1614, H1617–H1618, H1621–H1622, H1625–H1626, H1629–H1630, H1633–H1634, H1637–H1638, H1641–H1642, H1645–H1646, H1649–H1650, H1653–H1654, H1657–H1658, H1661–H1662, H1665–H1666, H1669–H1670, H1673–H1674, H1677–H1678, H1681–H1682, H1685–H1686, H1689–H1690, H1693–H1694, H1697–H1698, H1701–H1702, H1705–H1706, H1709–H1710, H1713–H1714, H1717–H1718, H1721–H1722, H1725–H1726, H1729–H1730, H1733–H1734, H1737–H1738, H1741–H1742, H1745–H1746, H1749–H1750, H1753–H1754, H1757–H1758, H1761–H1762, H1765–H1766, H1769–H1770, H1773–H1774, H1777–H1778, H1781–H1782, H1785–H1786, H1789–H1790, H1793–H1794, H1797–H1798, H1801–H1802, H1805–H1806, H1809–H1810, H1813–H1814, H1817–H1818, H1821–H1822, H1825–H1826, H1829–H1830, H1833–H1834, H1837–H1838, H1841–H1842, H1845–H1846, H1849–H1850, H1853–H1854, H1857–H1858, H1861–H1862, H1865–H1866, H1869–H1870, H1873–H1874, H1877–H1878, H1881–H1882, H1885–H1886, H1889–H1890, H1893–H1894, H1897–H1898, H1901–H1902, H1905–H1906, H1909–H1910, H1913–H1914, H1917–H1918, H1921–H1922, H1925–H1926, H1929–H1930, H1933–H1934, H1937–H1938, H1941–H1942, H1945–H1946, H1949–H1950, H1953–H1954, H1957–H1958, H1961–H1962, H1965–H1966, H1969–H1970, H1973–H1974, H1977–H1978, H1981–H1982, H1985–H1986, H1989–H1990, H1993–H1994, H1997–H1998, H2001–H2002, H2005–H2006, H2009–H2010, H2013–H2014, H2017–H2018, H2021–H2022, H2025–H2026, H2029–H2030, H2033–H2034, H2037–H2038, H2041–H2042, H2045–H2046, H2049–H2050, H2053–H2054, H2057–H2058, H2061–H2062, H2065–H2066, H2069–H2070, H2073–H2074, H2077–H2078, H2081–H2082, H2085–H2086, H2089–H2090, H2093–H2094, H2097–H2098, H2101–H2102, H2105–H2106, H2109–H2110, H2113–H2114, H2117–H2118, H2121–H2122, H2125–H2126, H2129–H2130, H2133–H2134, H2137–H2138, H2141–H2142, H2145–H2146, H2149–H2150, H2153–H2154, H2157–H2158, H2161–H2162, H2165–H2166, H2169–H2170, H2173–H2174, H2177–H2178, H2181–H2182, H2185–H2186, H2189–H2190, H2193–H2194, H2197–H2198, H2201–H2202, H2205–H2206, H2209–H2210, H2213–H2214, H2217–H2218, H2221–H2222, H2225–H2226, H2229–H2230, H2233–H2234, H2237–H2238, H2241–H2242, H2245–H2246, H2249–H2250, H2253–H2254, H2257–H2258, H2261–H2262, H2265–H2266, H2269–H2270, H2273–H2274, H2277–H2278, H2281–H2282, H2285–H2286, H2289–H2290, H2293–H2294, H2297–H2298, H2301–H2302, H2305–H2306, H2309–H2310, H2313–H2314, H2317–H2318, H2321–H2322, H2325–H2326, H2329–H2330, H2333–H2334, H2337–H2338, H2341–H2342, H2345–H2346, H2349–H2350, H2353–H2354, H2357–H2358, H2361–H2362, H2365–H2366, H2369–H2370, H2373–H2374, H2377–H2378, H2381–H2382, H2385–H2386, H2389–H2390, H2393–H2394, H2397–H2398, H2401–H2402, H2405–H2406, H2409–H2410, H2413–H2414, H2417–H2418, H2421–H2422, H2425–H2426, H2429–H2430, H2433–H2434, H2437–H2438, H2441–H2442, H2445–H2446, H2449–H2450, H2453–H2454, H2457–H2458, H2461–H2462, H2465–H2466, H2469–H2470, H2473–H2474, H2477–H2478, H2481–H2482, H2485–H2486, H2489–H2490, H2493–H2494, H2497–H2498, H2501–H2502, H2505–H2506, H2509–H2510, H2513–H2514, H2517–H2518, H2521–H2522, H2525–H2526, H2529–H2530, H2533–H2534, H2537–H2538, H2541–H2542, H2545–H2546, H2549–H2550, H2553–H2554, H2557–H2558, H2561–H2562, H2565–H2566, H2569–H2570, H2573–H2574, H2577–H2578, H2581–H2582, H2585–H2586, H2589–H2590, H2593–H2594, H2597–H2598, H2601–H2602, H2605–H2606, H2609–H2610, H2613–H2614, H2617–H2618, H2621–H2622, H2625–H2626, H2629–H2630, H2633–H2634, H2637–H2638, H2641–H2642, H2645–H2646, H2649–H2650, H2653–H2654, H2657–H2658, H2661–H2662, H2665–H2666, H2669–H2670, H2673–H2674, H2677–H2678, H2681–H2682, H2685–H2686, H2689–H2690, H2693–H2694, H2697–H2698, H2701–H2702, H2705–H2706, H2709–H2710, H2713–H2714, H2717–H2718, H2721–H2722, H2725–H2726, H2729–H2730, H2733–H2734, H2737–H2738, H2741–H2742, H2745–H2746, H2749–H2750, H2753–H2754, H2757–H2758, H2761–H2762, H2765–H2766, H2769–H2770, H2773–H2774, H2777–H2778, H2781–H2782, H2785–H2786, H2789–H2790, H2793–H2794, H2797–H2798, H2801–H2802, H2805–H2806, H2809–H2810, H2813–H2814, H2817–H2818, H2821–H2822, H2825–H2826, H2829–H2830, H2833–H2834, H2837–H2838, H2841–H2842, H2845–H2846, H2849–H2850, H2853–H2854, H2857–H2858, H2861–H2862, H2865–H2866, H2869–H2870, H2873–H2874, H2877–H2878, H2881–H2882, H2885–H2886, H2889–H2890, H2893–H2894, H2897–H2898, H2901–H2902, H2905–H2906, H2909–H2910, H2913–H2914, H2917–H2918, H2921–H2922, H2925–H2926, H2929–H2930, H2933–H2934, H2937–H2938, H2941–H2942, H2945–H2946, H2949–H2950, H2953–H2954, H2957–H2958, H2961–H2962, H2965–H2966, H2969–H2970, H2973–H2974, H2977–H2978, H2981–H2982, H2985–H2986, H2989–H2990, H2993–H2994, H2997–H2998, H3001–H3002, H3005–H3006, H3009–H3010, H3013–H3014, H3017–H3018, H3021–H3022, H3025–H3026, H3029–H3030, H3033–H3034, H3037–H3038, H3041–H3042, H3045–H3046, H3049–H3050, H3053–H3054, H3057–H3058, H3061–H3062, H3065–H3066, H3069–H3070, H3073–H3074, H3077–H3078, H3081–H3082, H3085–H3086, H3089–H3090, H3093–H3094, H3097–H3098, H3101–H3102, H3105–H3106, H3109–H3110, H3113–H3114, H3117–H3118, H3121–H3122, H3125–H3126, H3129–H3130, H3133–H3134, H3137–H3138, H3141–H3142, H3145–H3146, H3149–H3150, H3153–H3154, H3157–H3158, H3161–H3162, H3165–H3166, H3169–H3170, H3173–H3174, H3177–H3178, H3181–H3182, H3185–H3186, H3189–H3190, H3193–H3194, H3197–H3198, H3201–H3202, H3205–H3206, H3209–H3210, H3213–H3214, H3217–H3218, H3221–H3222, H3225–H3226, H3229–H3230, H3233–H3234, H3237–H3238, H3241–H3242, H3245–H3246, H3249–H3250, H3253–H3254, H3257–H3258, H3261–H3262, H3265–H3266, H3269–H3270, H3273–H3274, H3277–H3278, H3281–H3282, H3285–H3286, H3289–H3290, H3293–H3294, H3297–H3298, H3301–H3302, H3305–H3306, H3309–H3310, H3313–H3314, H3317–H3318, H3321–H3322, H3325–H3326, H3329–H3330, H3333–H3334, H3337–H3338, H3341–H3342, H3345–H3346, H3349–H3350, H3353–H3354, H3357–H3358, H3361–H3362, H3365–H3366, H3369–H3370, H3373–H3374, H3377–H3378, H3381–H3382, H3385–H3386, H3389–H3390, H3393–H3394, H3397–H3398, H3401–H3402, H3405–H3406, H3409–H3410, H3413–H3414, H3417–H3418, H3421–H3422, H3425–H3426, H3429–H3430, H3433–H3434, H3437–H3438, H3441–H3442, H3445–H3446, H3449–H3450, H3453–H3454, H3457–H3458, H3461–H3462, H3465–H3466, H3469–H3470, H3473–H3474, H3477–H3478, H3481–H3482, H3485–H3486, H3489–H3490, H3493–H3494, H3497–H3498, H3501–H3502, H3505–H3506, H3509–H3510, H3513–H3514, H3517–H3518, H3521–H3522, H3525–H3526, H3529–H3530, H3533–H3534, H3537–H3538, H3541–H3542, H3545–H3546, H3549–H3550, H3553–H3554, H3557–H3558, H3561–H3562, H3565–H3566, H3569–H3570, H3573–H3574, H3577–H3578, H3581–H3582, H3585–H3586, H3589–H3590, H3593–H3594, H3597–H3598, H3601–H3602, H3605–H3606, H3609–H3610, H3613–H3614, H3617–H3618, H3621–H3622, H3625–H3626, H3629–H3630, H3633–H3634, H3637–H3638, H

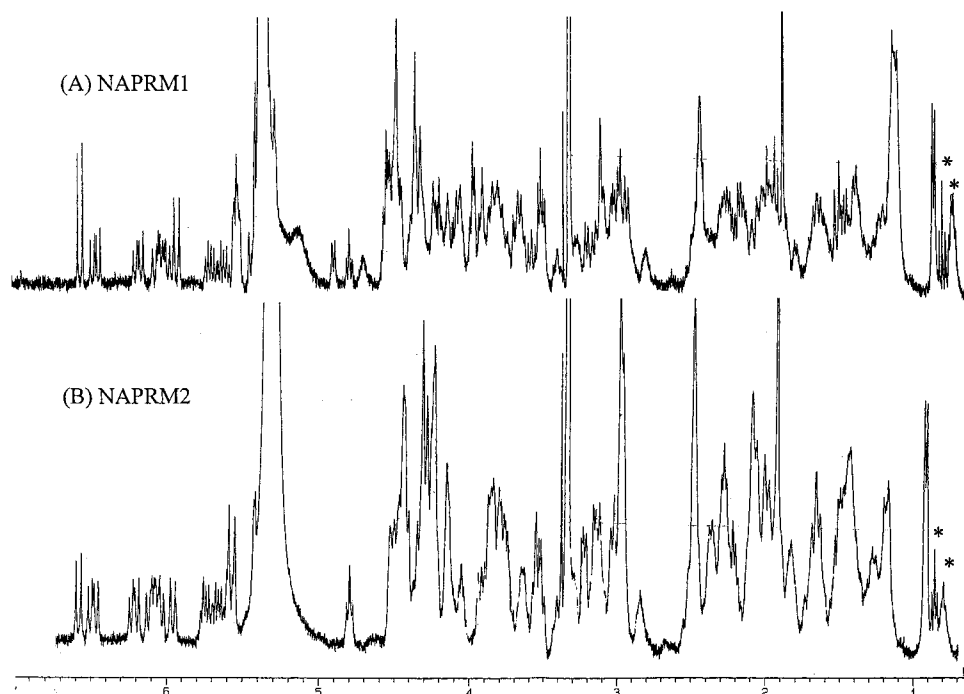


**Figure 3.**  $^1\text{H}$  NMR spectra of NAPRM1 (top) and NAPRM2 (bottom). The spectra were measured in  $\text{CD}_3\text{OD}/\text{C}_5\text{D}_5\text{N}$  (1:1) at 400 MHz. The symbol \* signifies impurities.

**Table 1.**  $^1\text{H}$  and  $^{13}\text{C}$  NMR Assignments of NAPRM2 in  $\text{CD}_3\text{OD}/\text{C}_5\text{D}_5\text{N}$  (1:1)

postn	$^{13}\text{C}^a$	$^1\text{H}^b$												
1	131.8	6.54	19	134.0	5.54	34	76.2	3.76	48	66.7	4.19	64	30.8	1.32
2	116.1	5.92	20	79.5	3.81	35	32.4	1.37	49	82.2	2.98	81	76.2	4.10
3	78.5		21	33.3	1.36			2.02	50	71.1	3.73	65	78.1	2.93
4	93.6				1.62	36	30.9	1.23	51	41.4	1.60	66	81.0	3.52
5	21.0	2.43	22	31.2	1.42			1.94			2.42	67	75.0	3.79
6	21.5	2.45			1.90	37	77.9	3.07	52	67.8	3.59	68	71.2	4.39
7	92.5		23	79.8	2.92	38	84.4	3.12	53	85.6	3.46	69	78.2	3.85
8	82.8		24	79.0	3.06	39	31.6	2.04	54	74.2	4.43	70	73.6	4.42
9	112.0	5.52	25	37.8	1.47	40	38.5	1.44	55	35.8	2.03	71	71.4	4.27
10	143.0	6.45			2.25			1.67			2.47	72	73.6	4.27
11	134.1	6.06	26	78.9	2.95	41	76.7	3.10	56	60.3	4.48	73	71.5	3.89
12	135.0	5.70	27	78.9	3.01	42	81.3	2.80	57	80.7	3.19	74	75.2	4.19
13	39.3	2.16	28	39.8	1.44	43	31.2	1.38	58	69.6	4.24	75	37.8	1.85
		2.22			2.32			1.86	59	38.7	1.59			2.34
14	51.0	4.02	29	78.1	4.09	44	29.2	1.38			2.23	76	70.7	4.33
15	39.3	2.17	30	82.6	3.37			1.77	60	66.2	4.23	77	88.0	3.76
		2.23	31	39.1	2.05	45	82.0	3.26	61	84.9	3.20	78	70.9	4.39
16	132.6	5.62			2.32	46	76.0	3.82	62	77.4	3.62	79	37.3	1.93
17	134.5	6.01	32	72.7	4.10	47	36.6	1.61	63	30.3	1.22			2.07
18	133.0	6.18	33	86.9	2.93			2.02			1.96	80	72.0	4.45

<sup>a</sup>  $^{13}\text{CD}_3\text{OD}$  was adjusted to 50.0 ppm in  $\text{CD}_3\text{OD}-\text{C}_5\text{D}_5\text{N}$  (1:1) at 125 MHz except for C90. <sup>b</sup>  $\text{CD}_2\text{HOD}$  was adjusted to 3.31 ppm in  $\text{CD}_3\text{OD}/\text{C}_5\text{D}_5\text{N}$  (1:1) at 400 MHz. <sup>c</sup> Denotes each assignment is interchangeable. <sup>d</sup>  $1,4^{13}\text{CD}_8\text{O}_2$  was adjusted to 67.8 ppm in dioxan-*d*<sub>8</sub>/ $\text{D}_2\text{O}/\text{CD}_3\text{COOD}$  (10:10:1) at 125 MHz.

newly separated H61 signal ( $\delta$  3.24  $J = 8.5$ , 2 Hz) measured in the latter solvent. The proton connectivity was interrupted at H71. Because of the equatorial disposition on a chair-type oxane, H71 showed a very small coupling constant with H71 and H72. Furthermore, the closeness of chemical shift between H71 and H72 made it difficult to distinguish the two protons. The spin system was also disconnected between H82 and H83 because of the small coupling constant due to a dihedral angle of almost 90 degrees. These interrupted proton connectivities were resolved by cross-peaks of H70/C71, H71/C70, H71/C72, and H83/C82, respectively, in the HMBC spectrum of NAPRM2.

The  $^{13}\text{C}$  NMR chemical shifts for prymnesin-2 (Table 1) were assigned with NAPRM2 (unless otherwise stated).<sup>14</sup> The  $^{13}\text{C}$ -

$^1\text{H}$  correlation NMR spectra (HSQC and HMBC) were mainly used because of the incomplete resolution for the  $^1\text{H}$ -dimension and poor signal-to-noise ratios for  $^{13}\text{C}$  observed NMR data (broad-band proton-decoupled and DEPT135). Among the protonated carbons in NAPRM2, C1 and C90 in NAPRM2 could not be assigned by HSQC measurement. For C1, this was explained by the actual coupling constant for  $^1J_{\text{C1-H1}}$  (200 Hz),<sup>15</sup> which was too large to be detected under ordinary experimental condition for  $^1J_{\text{C-H}}$  (120 Hz). The coupling constant of 200 Hz

(14) Carbons of NAPRM2 comprised 2 methyls, 24 methylenes, 10 olefinic methines, 54 other methines, and 8 quaternary carbons.

(15) Since the  $\text{sp}^2$  carbon of C1 possesses a chlorine atom, the coupling constant of C1-H1 should be approximately 200 Hz as described in Levy, G. C.; Nelson, G. L. *Carbon-13 Nuclear Magnetic Resonance for Organic Chemists*; John Wiley & Sons: New York, 1972; p 69.

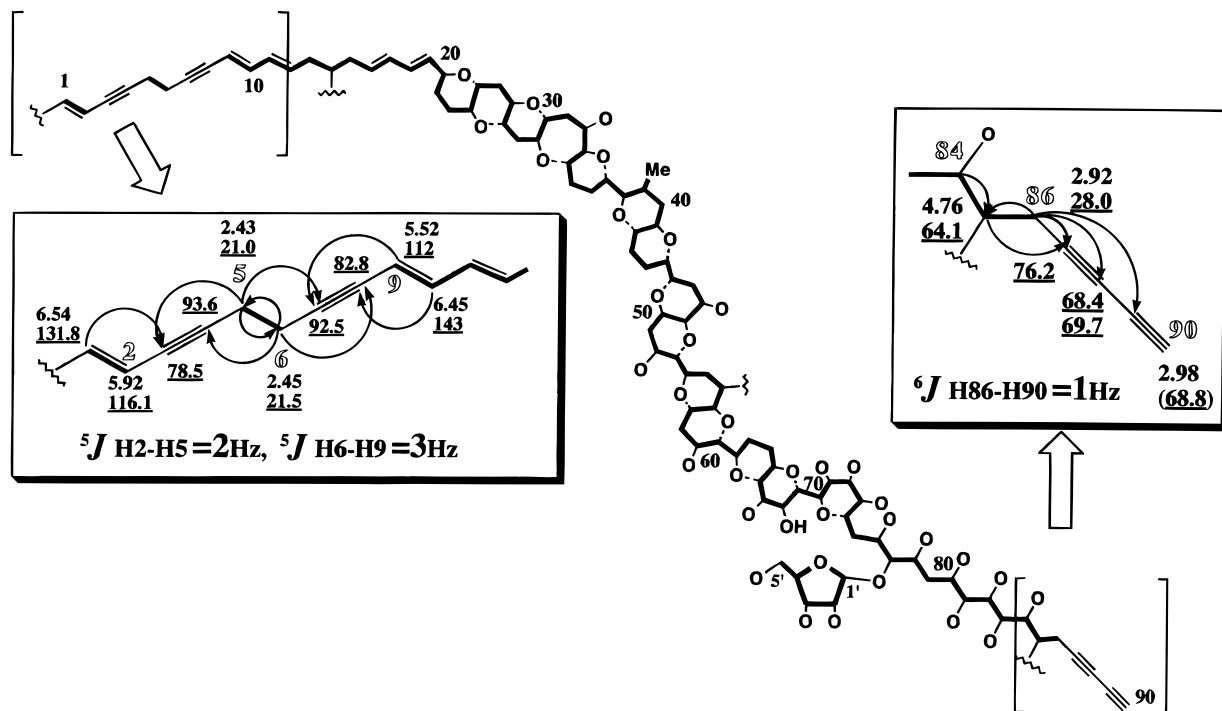


**Figure 4.** Structural elucidation of both termini of PRM2 by HMBC and chemical shifts. The arrows denote long-range correlations between protons (tail) and carbons (head) shown in HMBC. Normal and underlined numbers indicate the proton and carbon chemical shifts, respectively.

for  $^1J_{C1-H1}$  calculated from the split cross-peak in the HMBC spectrum<sup>16</sup> suggested that C1 bore a chlorine atom. Another carbon, C90, located at the terminus of conjugated triple bonds was undetectable by  $^1H$ -detected HSQC experiment with the basic solvent  $CD_3OD/C_5D_5N$  (1:1).<sup>17</sup> Consequently, replacement of H90 with deuterium was suspected. When the solvent was changed to an acidic one  $CD_3OD/CD_3COOD$  (19:1), the H90 signal became clearly detectable at  $\delta$  2.63 as a broad singlet ( $J = 1.2$ , t) in the COSY spectrum of PRM2. The chemical shift of C90 ( $\delta$  68.8) was determined by HSQC of NAPRM2 in another acidic solvent [1,4-dioxan- $d_8$ /D $_2$ O/ $CD_3COOD$  (10:10:1)]. The HMBC data disclosed the presence of four elusive quaternary carbons in the beginning section (C1–C10) of the molecule (Figure 4). HMBC correlations to all quaternary carbon were as follows; C3 ( $\delta$  78.5) versus H1 and H5, C4 ( $\delta$  93.6) versus H6, C7 ( $\delta$  92.5) versus H5 and H9, and C8 ( $\delta$  82.8) versus H6 and H10. Characteristic chemical shifts, such as upfield values for C2 ( $\delta$  116), C9 ( $\delta$  112) and those for equivalent two methylenes (H25 and H26  $\delta$  2.47, C5 and C6  $\delta$  21), could be accounted for by a bis-conjugated enyne system. The triconjugated enyne-diene system from C7 to C12 was supported by the UV maxima data 244, 267, 278 nm.<sup>18</sup> The section from C1 to C5 was supported by comparable chemical shifts and coupling constants reported for a similar structure.<sup>19</sup> After extensive analyses of HMBC and  $^{13}C$  NMR data, three unassignable quaternary carbons ( $\delta$  76.2, 68.4, 69.7) were left beyond C86 (Figure 4). Cross-peaks in the HMBC spectrum (H85/C87, H86/C88, H86/C89) clarified three quaternary carbons, though assignment of C88 ( $\delta$  68.4) and C89 ( $\delta$  69.7) could

(16) As shown in the Supporting Information, a pair of cross-peaks was observed at the  $^{13}C$  level of 131.8 ppm in the HMBC spectrum of NAPRM2. The midpoint of the two peaks was just on the proton axis of  $\delta$  H1 (6.58 ppm), enabling us to determine  $\delta$  C1 at 131.8 ppm and to calculate the coupling constant of  $^1J_{C1-H1}$  at 200 Hz, based on the split peak width.

(17) Disappearance of the H90 signal ( $\delta$  2.98) due to substitution with D occurred in 12 h as demonstrated in the Supporting Information of the previous contribution.<sup>7</sup>

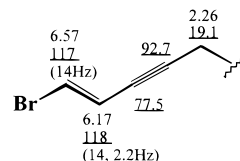
(18) Georjieff, K. K.; Cave, W. T.; Blaikie, K. G. *J. Am. Chem. Soc.* **1954**, *76*, 5494–5499.

be exchangeable. As noted previously, dehydrochlorination of NAPRM2 was presumed to occur at chlorine on C85 and H86. The acidity of the methylene protons could be explained if they were adjacent to a diyne structure. After the disappearance of the proton signals of H85 ( $\delta$  4.76) and H86 ( $\delta$  2.92) by dehydrochlorination, two proton signals (H85  $\delta$  6.97, H86  $\delta$  6.05)<sup>20</sup> appeared in the conjugated double bond region, supporting that the terminal moiety was a conjugated diyne system.<sup>21</sup>

Changes in the chemical shift after *N*-acetylation of PRM2 are shown in Tables 1 and 2. Considering the large anisotropic effect induced by the carbonyl group, both a large downfield shift of H14 by 0.7 ppm and fairly large upfield shifts of H13a,b and H15a,b by 0.2–0.25 ppm strongly suggested that the amino group was located at C14.

The protons from H1' to H5' was previously assigned to those on a sugar moiety,<sup>7</sup> based on an isolated acetal H1' signal ( $\delta$  5.4, d, 3.8 Hz), geminal coupling of oxymethylene H25' ( $\delta$  3.68, 3.73, dd 4, 13 Hz), and continuous oxymethines from H2' to H4'. The HMBC correlations for H1'/C5' and H1'/C77 revealed that the sugar was a pentofuranose and the glycosidic bond was

(19) The chemical shifts ( $\delta$  H and  $\delta$  C) and coupling constants shown below were described in the literature; Hirsh, S.; Carmely, S.; Kashman, Y. *Tetrahedron* **1987**, *43*, 3257–3261.



(20) The proton numbers in parentheses indicate the positions after the dehydrochlorination.

(21) The long-range coupling constant of 1.2 Hz between H86 and H90 well matched the literature value; Joure, M. P.; Simonnin, M. P. *Compt. Rend.* **1963**, *257*, 121. If the number of triple bonds exceeded three, the coupling constant should be less than 0.6 Hz. Absence of additional quaternary carbons in the range  $\delta$  60–100 further supports the proposed terminal structure.

**Table 2.**  $^1\text{H}$  NMR Assignments of Prymnesin-2<sup>a</sup>

postn	$^1\text{H}$										
1	6.58	19	5.64	34	3.65	48	4.14	64	1.53	81	3.74
2	5.95	20	3.94	35	1.42	49	2.99		2.13	82	3.83
3		21	1.50		2.07	50	3.58	65	3.04	83	3.96
4			1.83	36	1.34	51	1.45	66	3.33	84	3.93
5	2.52	22	1.51		2.03		2.30	67	3.63	85	4.50
6	2.54		2.03	37	3.17	52	3.49	68	4.04	86	2.88
7		23	3.04	38	3.19	53	3.29	69	3.55	87	
8		24	3.15	39	2.26	54	4.27	70	3.99	88	
9	5.63	25	1.44	40	1.63	55	2.04	71	3.94	89	
10	6.50		2.23		1.82		2.40	72	3.93	90	2.63
11	6.26	26	3.00	41	3.18	56	4.50	73	3.57	91Me	0.98
12	5.72	27	3.07	42	2.95	57	3.32	74	3.80	1'	5.25
13	2.43	28	1.35	43	1.44	58	4.06	75	1.62	2'	4.14
	2.45		2.27		1.94	59	1.65		2.03	3'	4.03
14	3.32	29	3.90	44	1.44		2.19	76	4.10	4'	4.20
15	2.40	30	3.36		1.85	60	4.22	77	3.63	5'	3.61
	2.43	31	1.94	45	3.30	61	3.24	78	4.17		3.68
16	5.62		2.35	46	3.67	62	3.53	79	1.67		
17	6.20	32	4.03	47	1.63	63	1.30		1.85		
18	6.28	33	2.98		1.93		2.07	80	4.09		

<sup>a</sup> Chemical shifts are measured in  $\text{CD}_3\text{OD}/\text{CD}_3\text{COOD}$  (19:1). <sup>b</sup>  $\text{CD}_2\text{HOD}$  was taken as a standard peak at  $\delta$  3.31.

at C77. The sugar was finally identified as L-xylose by GC analysis with a chiral column of the trifluoroacetate of the hydrolyzed products of PRM2.<sup>22</sup> The  $\alpha$ -anomeric glycosidic bond was determined by comparison of the chemical shifts and coupling constants with literature values.<sup>23</sup>

The locations of ether linkages were determined basically by NOESY experiments of NAPRM2. Negative NOEs originating from 1,3-diaxial protons residing at both sides of a cyclic ether were prominently shown in the spectra.<sup>24</sup> All of the angular protons interposing ether oxygens, except for H49/H53 (ring I), gave rise to clear cross-peaks in the NOESY spectra of

(22) The procedure for trifluoroacetylation and GC analyses basically followed the method of Matsunaga, S.; Fusetani, N.; Kato, Y. *J. Am. Chem. Soc.* **1991**, *113*, 9690–9692.

(23) The chemical shifts and coupling constants for the sugar moiety in NAPRM2 are as follows: C1' ( $\delta$  106.2, 5.38, d,  $J = 4$  Hz), C2' ( $\delta$  74.6, 4.20), C3' ( $\delta$  72.8, 4.18), C4' ( $\delta$  88.2, 4.41), and C5' ( $\delta$  64.5, 3.68, 3.73, dd,  $J = 4, 13$  Hz). Using the  $^{13}\text{C}$  NMR data for monosaccharides in the literature,<sup>23</sup> we could determine that the pentose was a furanoside. From the coupling constant of 4 Hz for  $J_{\text{H1-H2}}$ , we could determine that the glycosidic bond is an  $\alpha$ -anomer.<sup>23b,c</sup> Referenced NMR data are given below: (a)  $^{13}\text{C}$  NMR in Bock, K.; Pedersen, C. Carbon-13 nuclear magnetic resonance spectroscopy of monosaccharides. In *Advances in Carbohydrate Chemistry and Biochemistry*; Academic Press: 1983; Vol. 41, pp 27–66:  $\alpha$ -xylofuranoside C1 ( $\delta$  103.0), C2 (77.8), C3 (76.2), C4 (79.3), C5 (61.6);  $\beta$ -xylofuranoside C1 (109.7), C2 (81.0), C3 (76.0), C4 (83.6), C5 (62.2);  $\alpha$ -ribofuranoside C1 (103.1), C2 (71.1), C3 (69.8), C4 (84.6), C5 (61.9);  $\beta$ -ribofuranoside C1 (108.0), C2 (74.3), C3 (70.9), C4 (83.0), C5 (62.9);  $\alpha$ -xylopyranoside C1 (100.6), C2 (72.3), C3 (74.3), C4 (70.4), C5 (62.0);  $\beta$ -xylopyranoside C1 (105.1), C2 (74.0), C3 (76.9), C4 (70.4), C5 (66.3);  $\alpha$ -ribofuranoside C1 (100.4), C2 (69.2), C3 (70.4), C4 (67.4), C5 (60.8);  $\beta$ -ribofuranoside C1 (103.1), C2 (71.0), C3 (68.6), C4 (68.6), C5 (63.9). (b)  $^1\text{H}$  NMR and  $J_{\text{H1-H2}}$  in Rudrum, M.; Shaw, D. F. *J. Am. Chem. Soc.* **1965**, *52*.  $\alpha$ -Xylofuranose H1 ( $\delta$  5.39,  $J_{\text{H1-H2}} = 4.0$  Hz),  $\beta$ -xylofuranose H1 (5.19,  $J_{\text{H1-H2}}$  was not described),  $\alpha$ -ribofuranose H1 ( $\delta$  5.34, 3.0 Hz),  $\beta$ -ribofuranose H1 ( $\delta$  5.21, 1.7 Hz). (c)  $J_{\text{H1-H2}}$  in Steavens, J. D.; Fletcher, H. G., Jr. *J. Org. Chem.* **1968**, *33*, 1799–1805.  $\alpha$ -Xylofuranoseperbenzoate ( $J_{\text{H1-H2}} = 4.4$  Hz),  $\beta$ -xylofuranoseperbenzoate ( $J_{\text{H1-H2}} < 0.5$  Hz),  $\alpha$ -ribofuranoseperbenzoate ( $J_{\text{H1-H2}} = 4.3$  Hz),  $\beta$ -ribofuranoseperbenzoate ( $J_{\text{H1-H2}} < 0.5$  Hz).

(24) Intense cross-peaks except for vicinal and geminal correlations in the rings A–N in the NOESY of NAPRM2 (occasionally of PRM2) showed close distances of H20/H24, H20/H22b, H21a/H23, H22b/H24, H23/H25a, H23/H27, H24/H26, H25a/H27, H26/H28b, H26/H30, H27/H29, H28b/H30, H29/H31a, H29/H34, H31b/H33, H32/Me91, H33/H37, H33/H35b, H34/H36a, H35b/H37, H36a,b/H38, H37/H39, H38/H42, H39/Me91, H40a/Me91, H40b/H42, H41/Me91, H41/H43a, H41/H45, H42/H44b, H43a/H45, H44a/H46, H45/H47a, H46/H50, H47b/H49, H49/H51b, H49/H53, H50/H52, H51b/H53, H52/H54, H52/H55a,b, H54/H58, H55b/H57, H57/H59b, H57/H61, H59b/H61, H60/H62, H61/H63a,b, H62/H64a, H62/H66, H63b/H65, H64a/H66, H65/H67, H65/H69, H67/H69, H69/H71, and H70/H74.

NAPRM2 and NAPRM2-HCl. The ether bond for ring I was established in a different solvent,  $\text{CD}_3\text{OD}/\text{CD}_3\text{COOD}$  (19:1), by the NOE between H49 and H53 in the NOESY spectrum of PRM2. Based on the analyses of NOE and  $^{2,3}J_{\text{H-H}}$ , 14 ether rings from A to N were deduced to possess a sequence of 6/6/6/7/6–6/6–6/6–6/6–6/6–6. The first five rings (A–E) were shown to have *trans*-fused ladder-shaped structures, as is the case in dinoflagellate toxins such as ciguatoxin.<sup>25</sup> However, these NOE data alone were insufficient for complete verification of the ring sequence, especially that of repeating *trans*-1,6-dioxadecalin units. Therefore, in the following sections, we provide further details of the stereochemical structural assignments supported by a molecular mechanics calculation (MM2).<sup>26</sup>

The positions of hydroxyl groups were determined by comparing the  $^1\text{H}$  chemical shifts of NAPRM2 with those of peracetylpymnesin-2 (PAPRM2).<sup>27</sup> As shown in Figure 5 (also see Supporting Information), methine proton signals presumed to reside on hydroxy-bearing carbons were actually shifted downfield by 0.45–1.55 ppm, except for H56 and H85 in the spectrum of PAPRM2. Protons assigned to ether methines barely shifted downfield ( $< 0.3$  ppm).

Both an energy-dispersive X-ray analysis and the distribution of the cluster ions in the FAB mass spectrum implied that the NAPRM2 contained three chlorine atoms. The first chlorine at C1 has already been elucidated. The locations of the other two chlorine atoms were determined as follows. The second chlorine was deduced to reside on C56, since the carbon chemical shift of  $\delta$  60.3 was clearly separated at higher field from those of ether-bearing carbons ( $\delta$  69.6–88.0). In addition, no significant change in the chemical shift was observed for H56 after acetylation. Likewise, the last chlorine atom was assigned at

(25) Murata, M.; Legrand, A. M.; Ishibashi, Y.; Fukui, M.; Yasumoto, T. *J. Am. Chem. Soc.* **1990**, *112*, 4381–4386.

(26) Energy calculations of the rotamers and ring conformations were carried out with molecular mechanics using Allinger's parameters: (a) Werz, D. H.; Allinger, N. L. *Tetrahedron* **1979**, *35*, 3. (b) Allinger, N. L. *J. Am. Chem. Soc.* **1977**, *99*, 8127.

(27) We first measured  $^1\text{H}$  NMR spectra ( $^1\text{H}$ – $^1\text{H}$  COSY, HOHAHA, and NOESY) of PAPRM2 in  $\text{CD}_3\text{OD}/\text{C}_5\text{D}_5\text{N}$  (1:1) in order to compare the data with those of NAPRM2 under the same conditions. However, insufficient solubility after acetylation prevented us from complete signal assignments. The assignments were established by measuring the  $^1\text{H}$  NMR data ( $^1\text{H}$ – $^1\text{H}$  COSY, TOCSY, ROESY, and NOESY at 500 MHz) of PAPRM2 in  $\text{CD}_3\text{CN}/\text{D}_2\text{O}$  (8:2), which provided a better solubility for the peracetate.

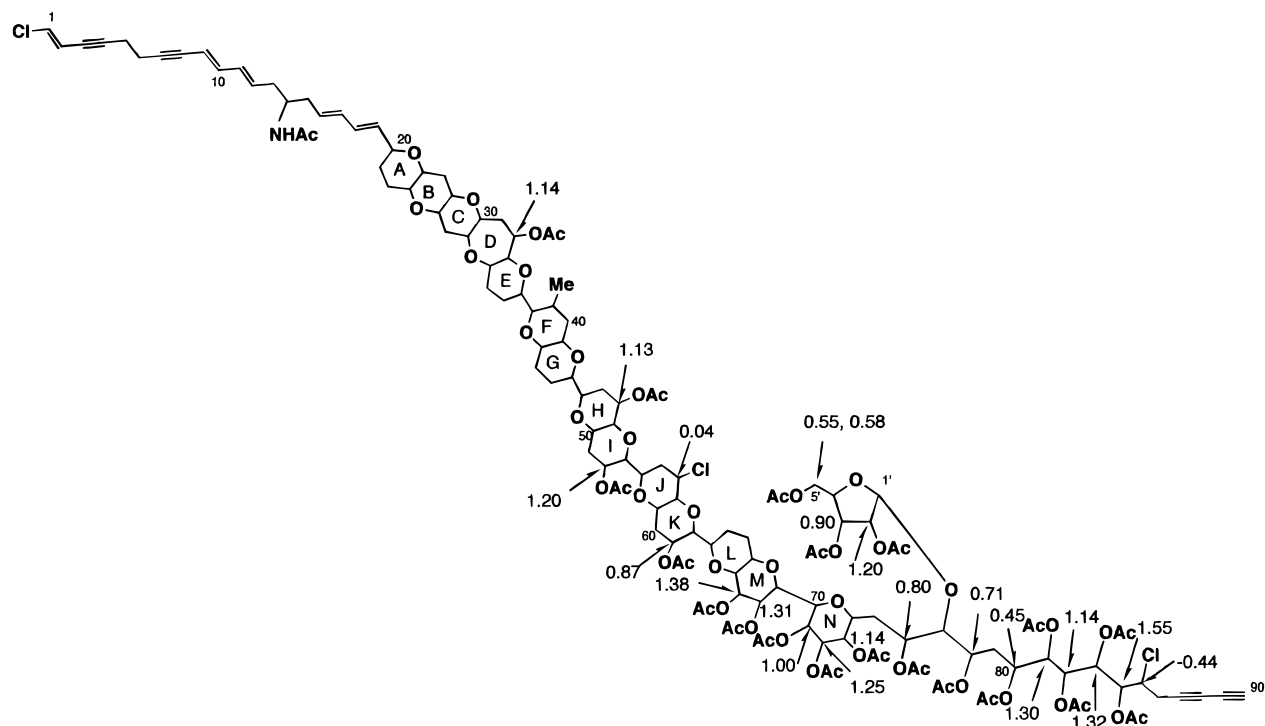


**Figure 5.** Downfield shifts of methine (methylene) protons after per-acetylation, confirming that these protons reside on carbons bearing hydroxyl groups. Chemical shifts are those in  $\text{CD}_3\text{OD}/\text{C}_5\text{D}_5\text{N}$  (1:1). Downfield shifts for protons at nonacetylated positions except for C14, were less than 0.2 ppm.

C85; no downfield shift was observed for H85 after acetylation and the carbon chemical shift of  $\delta$  64.1 was too far upfield for an ether-oxygenated methine. The assignment was also supported by the dehydrochlorination for chlorine on C85 and H86, as suggested by ESI-MS and  $^1\text{H}$  NMR data.

The unsaturated segments, particularly for polyacetylenic groups, were difficult to determine by NMR data alone, due to the paucity of protons. Hence, for further verification of the proposed structure, perhydropymnesin-2 (HPRM2) was prepared and subjected to MS and NMR analyses. Though the molecular weight should have increased from 1971 to 1997 by hydrogenation, the positive ESI-MS spectrum of HPRM2 showed pseudomolecular cluster ions at around  $m/z$  1963, 34 mass unit smaller than expected. Apparently dechlorination took place during hydrogenation. The isotopic distribution data simulated for the composition  $\text{C}_{96}\text{H}_{164}\text{Cl}_2\text{NO}_{35}$  was nearly consistent with the observed pseudomolecular ion-distribution; i.e., 26 protons were added to PRM2. Thus the presence of four triple and five double bonds in the molecule<sup>28</sup> was confirmed. All results thus obtained pointed the planar structure for pymnesin-2 to **2**.

**Stereochemistry of Pymnesin-2.** As shown in Figure 1, PRM2 possesses 49 chiral centers in its aglycone backbone. In the present study, the relative configurations of 39 chiral centers in the cyclic parts from C20 to C74 were determined by combining  $^1\text{H}$  NOEs and  $^{2,3}J_{\text{H-H}}$  data. Based on very weak NOEs and large coupling constants<sup>29</sup> (9–12 Hz), which are both typical for 1,2-antiperiplanar protons, as well as the strong NOEs

due to 1,3-diaxial protons, all six-membered rings (A/B/C, E, F/G, H/I, J/K, L/M, and N) were found to have chair conformations. These data also indicated *trans-cisoid* fusion for rings A/B/C, F/G, H/I, J/K, L/M. Further, the NOEs and  $^{2,3}J_{\text{H-H}}$  data clarified the orientation C32 OH as  $\alpha$ , Me 91 as  $\alpha$ , C48 OH as  $\alpha$ , C52 OH as  $\beta$ , chlorine on C56 as  $\alpha$ , C60 OH as  $\alpha$ , C67 OH as  $\alpha$ , C68 OH as  $\alpha$ , C71 OH as  $\beta$ , C72 OH as  $\alpha$  and C73 OH as  $\alpha$ . However, analogous with the K–L, O–P, and V–X ring junctures in maitotoxin,<sup>30</sup> assignment of the diastereomeric relations around the E–F, G–H, I–J, K–L, M–N rings in PRM2 was difficult by NOE due to possible rotation along the C–C axes connecting these rings. The proposed 6/6–6 sequence (e.g., rings F/G–H, H/I–J, J/K–L, or L/M–N) also appeared to be replaceable by a 6/7/7 system (described as an “alternative regio-isomer”)<sup>31</sup> without significant conflicts with the observed NOEs, coupling constants, or chemical shifts. Therefore the proposed ring sequence in these parts was rigorously tested with assistance of MM2 calculations. For effective MM2 calculations, the cyclic part of the molecule was divided into six segments (rings A–E, D–F, F–I, H–K, J–M, and L–N), where each of the latter five fragments contained a 2,2'-bistetrahydropyran juncture.

**Rings A–E.** In this ring sequence, the straightforward interpretation of NOEs and coupling constants was possible, since the rings from A to E formed a typical and rigid ladder-shaped polycyclic structure to show prominent 1,3-diaxial NOEs and large 1,2-antiperiplanar coupling constants. The possibility of conformational variation existed only in oxepane ring D. As shown in Figure 6a,b, two ring conformations were possible

(28) Due to insufficient signal-to-noise ratios, full assignments of the cross-peaks in the  $^1\text{H}$ – $^1\text{H}$  COSY and HOHAHA spectra of the perhydrogenated product were difficult. Therefore, we focused on the characteristic and intense cross-peaks arising from protons in the vicinity of the chlorine atoms, e.g., H54/H55, H56/H57, or H83/H84. Assignments of these signals were also supported by 1D NOE experiments. Thus, two chlorine atoms, on C56 and C85, respectively, were confirmed to remain in the molecule but the chlorine atom at C1 was substituted by a hydrogen during hydrogenation.

(29) The coupling constants were mainly calculated from the width of split signals. Isolated peaks were chosen from the  $^1\text{H}$ –1D spectra of PRM2, NAPRM2, and PPRM2.

(30) (a) Sasaki, M.; Matsumori, N.; Maruyama, T.; Nonomura, T.; Murata, M.; Tachibana, K.; Yasumoto, T. *J. Angew. Chem., Int. Ed. Engl.* **1996**, *35*, 5, 1672–1675. (b) Nonomura, T.; Sasaki, M.; Matsumori, N.; Maruyama, T.; Murata, M.; Tachibana, K.; Yasumoto, T. *J. Angew. Chem., Int. Ed. Engl.* **1996**, *35*, 1675–1678.

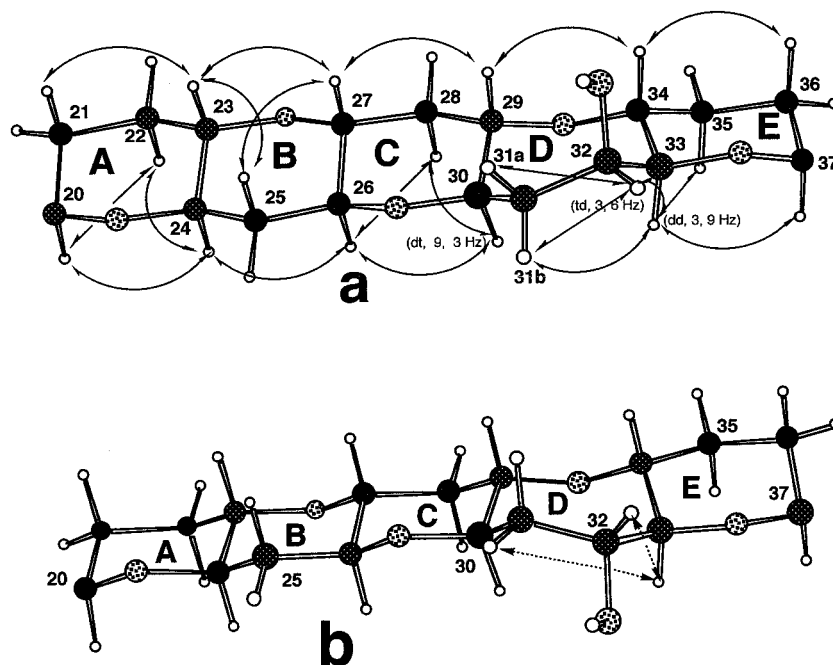


**Figure 6.** Two possible stereostructures for rings A–E based on NOEs and coupling constants; the proposed configuration (**a**) and the alternative one (**b**). In **a**, double-headed arrows denote NOEs chiefly detected in the NOESY of **2**. Coupling constants and multiplicities of the  $^1\text{H}$  signals (d, doublet; t, triplet) calculated from isolated signals in the 1D- $^1\text{H}$  NMR spectra of **1,2** or peracetylprymnesin-2, are shown in parentheses. In **b**, the observed NOEs (H32/H33 and H31b/H33) indicated with broken arrows could not be explained.

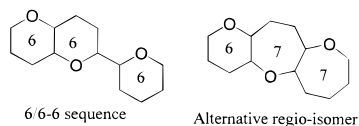
for the pseudoaxial orientation of C32 OH, both of which satisfied the intense NOEs for H31a,b/H32 and small coupling constant for H32/H33 (3 Hz). However, the observed NOEs for H31b/H33 and H32/H33 could not be explained by the 6b model. The proposed configuration (Figure 6a) was thus selected.

**Rings D–F.** Axial orientation for Me91 was clarified by the intense NOE between Me91 and H41 together with the small coupling constant for H38/H39 (2.5 Hz). Regarding the E/F linkage, the proposed model was deduced by the following relayed-NOEs. In addition to the obvious NOE for H33/H38, NOEs relayed through H37/H38 were confirmed between H42/H37 and H42/H33 in  $^1\text{H}$ -1D NOE spectrum. Thus the close proximity of H37 and H38 and linear alignment of H33–H37–H38–H42 was suggested (Figure 7a). The conventional *gauche* correlation for H37–C37–C38–H38 (Figure 7b) was ruled out on the basis of the 8.5 Hz coupling constant observed for H37/H38.<sup>32</sup> The *anti* rotamer (Figure 7c) was consistent with the large coupling constant but not with the strong NOE observed between H37–H38.<sup>33</sup> As a model satisfactory to both NOE and *J* data, we selected a twisted *gauche* rotamer for this junction, where two pairs of diaxial protons (H33 and H37, H38 and H42)

were aligned under approximately  $20^\circ$  of the dihedral angle (Figure 7a). Though this conformation best explained the observed data, a rather strong NOE observed for Me 91/H33 was still difficult to explain, as a greater than  $3.5 \text{ \AA}$  distance was suggested by this model. The presence of a minor *gauche* rotamer could explain this unexpected NOE.<sup>34</sup> For further verification, we must await a future chemical synthesis.

**Rings F–I.** The axial orientation for C48 OH was evident from the intense NOEs and small coupling constants (3 Hz) for both H47a,b/H48 and H48/H49. Additionally, a large coupling constant for H52/H53 (10 Hz) and a strong NOE for H50/H51 clearly indicated equatorial orientation for C52 OH. An intense NOE and small coupling constant between H45 and H46 (4.5 Hz) indicated that the predominant relative conformation of H45–C45–C46–H46 was *gauche*. The NOEs observed for both H45/H47a and H44a/H46 in addition to the absence of NOEs between H44a,b and H47a,b, led to the proposed conformer for rings G–H (Figure 8). Due to overlap of the signals for H43b and H44b, we could not determine, whether the dominant conformation of ring G was chair-type or boat-type by NOESY or ROESY spectra alone, as illustrated in the Supporting Information. To eliminate this ambiguity, we used

(31) As shown in the Supporting Information, we could easily rule out the alternative regio-isomers (6/7/7) for rings D–F, F–I, H–K, and J–M. The observed NOEs could not be explained by the distances for Me91/H32, H45/H46, H52/H55a,b, and H61/H63a, respectively.



On the other hand, due to the closeness of the chemical shifts, the alternative regio-isomer for rings L–N was difficult to reject. The ambiguity was clarified, however, by the NOE data of PAPRM2; NOEs observed for H68/H70 and H69/H71 in the ROESY spectrum of PAPRM2 fit the 6/6–6 model but disagreed with the large interproton distances ( $>3.77 \text{ \AA}$ ) in the 6/7/7 model. Similarly, lack of NOEs was inconsistent with the close proximity of the protons, H64/H71 ( $3.27 \text{ \AA}$ ) and H65/H71 ( $3.34 \text{ \AA}$ ) in the 6/7/7 model (see the Supporting Information of the previous contribution<sup>7</sup>).

(32) The coupling constant was determined from the signal width of H38 in both 1D NOE spectrum of NAPRM2 and  $^1\text{H}$ -1D spectrum of PAPRM2. The close chemical shifts of H37 ( $\delta$  3.08), H38 ( $\delta$  3.12), and H41 ( $\delta$  3.10), made it difficult to measure signal widths of H37 and H38. To solve the problem, signal enhancement by NOE in 1D experiment was applied. Irradiation at 2.80 ppm of the isolated H42 signal changed the signal shape of H38 to a doublet (8.5 Hz). In additional support, the H38 signal appeared as a distinct double doublet (8.5, 2.5 Hz), when protons at the bases of hydroxyl groups were shifted downfield by acetylation.

(33) In the diastereomer model shown in Figure 7c, the antiperiplanar configuration for H37/H38 could not explain the observed NOEs. The distances between H37/H42 and H38/H33 were also out of NOE range. The unobserved NOE for Me91/H37 was definitely inexplicable in view of their close distance (around  $2.5 \text{ \AA}$ ).

(34) The presence of an NOE for M91/H33 was determined from the HMQC-NOESY spectrum of NAPRM2 to avoid the proton signal overlap. Absence of the NOEs thus determined for Me91/H36a,b easily ruled out the twisted *gauche* rotamer in the alternative diastereomer.

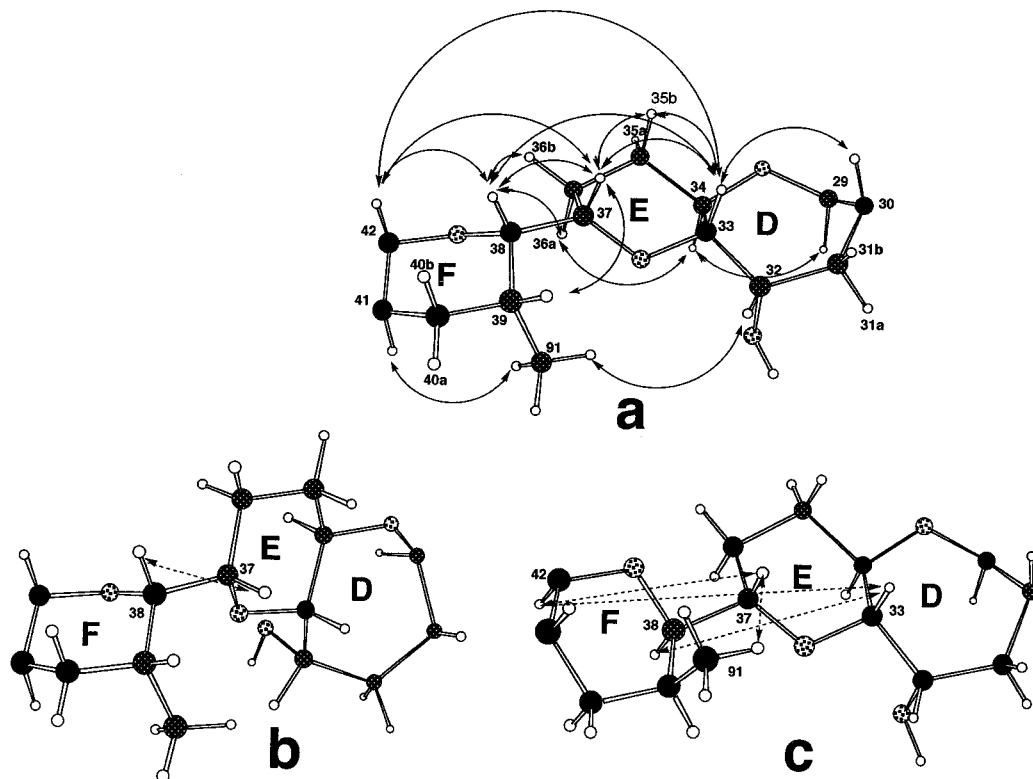


**Figure 7.** Three possible conformations for rings D–F, among which **a** was the proposed one. Alignment of protons was drawn to meet the strong relayed NOEs such as H33/H38, H37/H42. In **b** and **c**, broken arrows indicate inconsistency with the observed data. The observed coupling constant (8.5 Hz) is too large for the *gauche* conformation for H37/H38 in the **b** model, the observed NOEs for H33/H38, H33/H42, H37/H42 and unobserved NOE for Me 91/H37 are inconsistent with the distances for each of the protons in the **c** model.

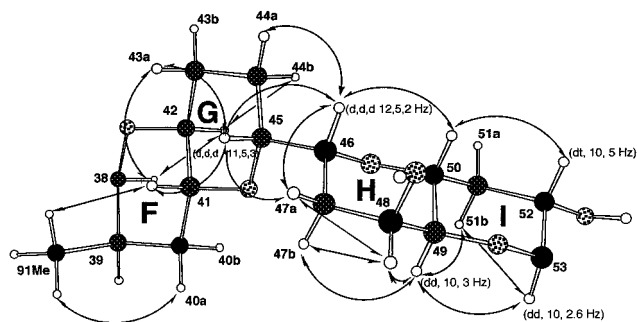


**Figure 8.** Stereostructure of rings F–I based on NOEs and coupling constants. Double-headed arrows indicate NOEs. Coupling constants and multiplicities of  $^1\text{H}$  signals are shown in parentheses.

the difference in carbon chemical shifts between C43 ( $\delta$  31.2) and C44 ( $\delta$  29.2) and conducted an HMQC–NOESY experiment of NAPRM2. An NOE found between H42 and H44 through C44 in the HMQC–NOESY spectrum was inconsistent with the distance between H42 and H44a,b (4.25, 4.28 Å) in the boat model of ring G. Thus G ring should be also in a chair conformation.

**Rings H–K.** Based on the intense NOEs for H55a,b/H56 and a small coupling constant for H56/H57 (3 Hz), chlorine on C56 was found to be axially substituted on ring J. *Gauche* conformation for H53/H54 was evident, since  $^3J_{\text{H53–H54}}$  2.6 Hz is typical for *gauche* and an intense NOE was observed between H53 and H54. The present rotamer satisfied prominent NOEs for H52/H55a,b and H52/H54 and a very weak NOE for H53/H55b (Figure 9a). However, as reported previously,<sup>35</sup> force-field calculations (Tripos,<sup>36</sup> MM2, CVFF<sup>37</sup>) suggested that the

*anti* conformation for H53–H54 is the overall state rotamer while the *gauche* conformation is energetically disfavored.<sup>38</sup> Therefore, the proposed rotamer was closely compared with two other *gauche* rotamers containing diastereomeric rings H–K. However, both alternative structures (Figure 9b,c) could be rejected for the following reasons. In the rotamer in Figure 9b, the distance between H55a and H52 (4.83 Å) definitely contradicted the strong NOE observed. The rotamer in Figure 9c was not consistent with the observed data. First, the NOE observed for H52/H54 is not possible considering their separation (3.93 Å). Second, the NOE detected for H55a/H52 was much stronger than that for H55b/H52 in the NOESY spectra of both NAPRM2 and PPRM2, which is not consistent with the distances of H55a/H52 (2.43 Å) and H55b/H52 (1.41 Å) for the rotamer in Figure 9c but is consistent with those for the proposed rotamer in Figure 9a (H55a/H52–2.51 Å, H55a/H52–3.34 Å). Moreover, in the NOESY spectrum of PRM2 measured in the acidic solution, the NOEs for H55a,b/H53 and H55b/H52 were not observed, while those for H53/H54 and H52/H54 were detected clearly. Thus the proposed rotamer was again supported (see Supporting Information).

**Rings J–M.** Coupling constants of 9 Hz for  $^3J_{\text{H66–H67}}$  and 1 Hz for  $^3J_{\text{H68–H69}}$  clearly indicated equatorial orientation for C67 OH and axial orientation for C68 OH. Judging from  $^3J_{\text{H61–H62}}$  8.5 Hz, together with the NOEs for H60/H62 and H61/H63a,b, the K–L juncture was inferred to have *anti* conforma-

(36) Clark, M.; Cramer, R. D.; Van Opdenbosch, N. *J. Comput. Chem.* **1989**, *10*, 982.

(37) Dauber-Osguthorpe, P.; Robert, V. A.; Dauber-Osguthorpe, D. J.; Wolff, J.; Genest, M.; Hagler, A. T. *Proteins: Struct., Func., Genet.* **1988**, *4*, 31.

(38) A weak NOE was observed for H53/H55a in the NOESY spectra of NAPRM2 and PRM2. Most probably, the intense NOE for H53/H54 was relayed to H55 in the proposed rotamer shown in Figure 9a.

(35) Glendenning, L.; Igarashi, T.; Yasumoto, T. *Bull. Chem. Soc. Jpn.* **1996**, *69*, 2253–2263.

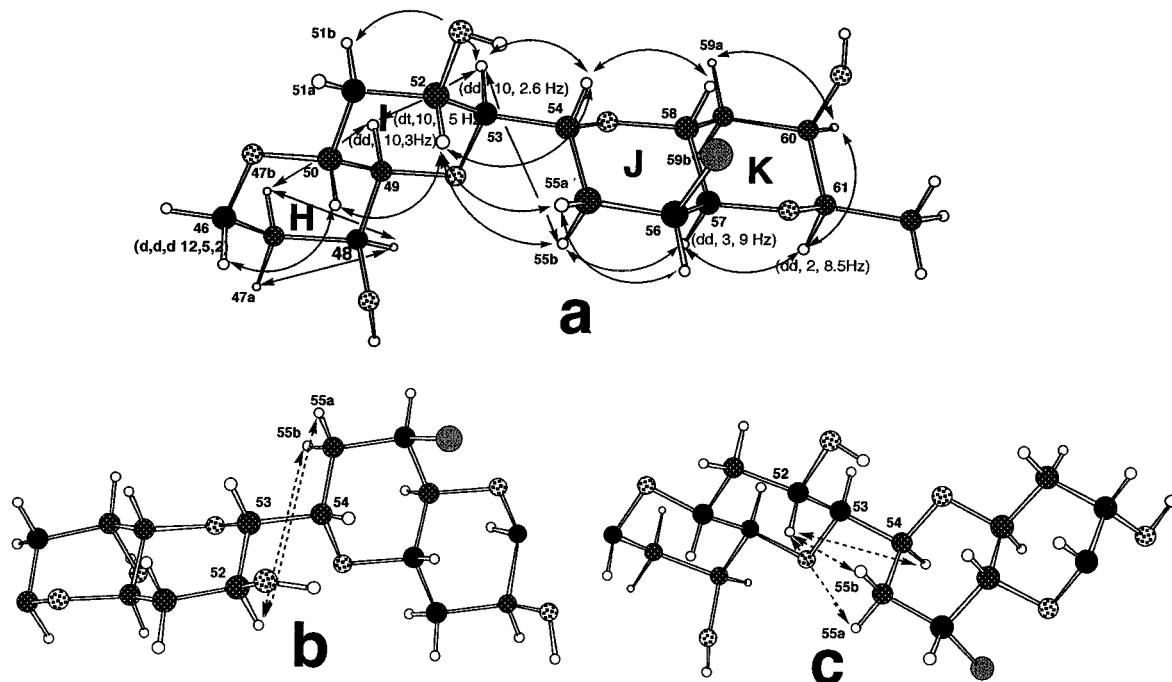


**Figure 9.** The proposed structure (a) and two possible diastereomers (b and c) for rings H–K. All of them conform to the NMR findings of a small coupling constant and a large NOE between H53 and H54.; **54 R\*** (a) and **54 S\*** (b, c). In b and c, observed data inexplicable by these models are indicated with broken arrows as follows; the observed NOEs for H52/H55a,b disagree with the distances for these protons in the b model, the observed NOEs for H52/H54, H52/H55a and unobserved or very weak NOE for H52/H55b were inconsistent with the distances expected from c model.

tion. Unlike rings I–J, the *anti* rotamer in the corresponding diastereomer could be ruled out by the absence of NOEs for H60/H63a,b, as they should be located in the proximate distance (2.54 Å, 3.00 Å) in this geometry. Hence, the proposed configuration should be selected for the stereostructure of rings J–M (Figure 10a).<sup>39</sup>

**Rings L–N.** As above structural assignment of the segment between rings M and N including their stereochemistry was the most difficult part to accomplish, since all carbons were oxygenated and thereby gave rise to methine signals with nearly identical chemical shifts. The signals became distinguishable only after peracetylation. As indicated in Figure 10b, the relative stereochemical correlation for rings M–N was also *anti*, based on the coupling constant of 9.5 Hz between H69 and H70 as determined by the line widths of H69 and H70 in the <sup>1</sup>H-1D spectra of NAPRM2 and PAPRM2. As with rings K–L, the alternative diastereomer was ruled out simply by the absence of NOE for H68/H71, since their interproton distance (2.49 Å) deduced from the MM2 calculation should be well within the NOE range. All of these data resulted in the assignment of the configurations of rings A–N (C20–C74) of PRM2. The configurations of C14 and C76–C85 remained undetermined.

**Structure of Prymnesin-1.** As discussed in the preceding sections, the <sup>1</sup>H-1D spectrum of PRM1 closely resembled that of PRM2. Therefore, we first compared the NMR data (COSY, TOCSY, and HMQC) of NAPRM1 measured at 500 MHz in CD<sub>3</sub>OD/C<sub>5</sub>D<sub>5</sub>N (1:1) with those of NAPRM2. The following two features stood out. First, the differences in the proton and

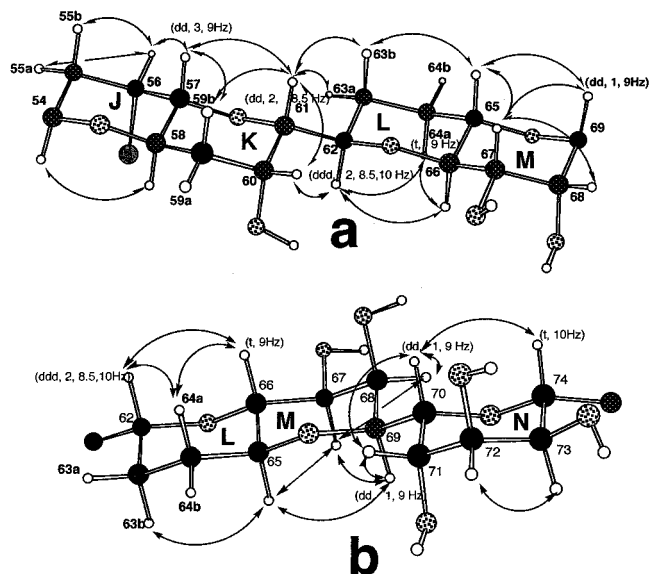


**Figure 10.** Stereostructures of rings J–M (a) and L–N (b) generated by MM2 calculations incorporating <sup>2,3</sup>J<sub>H–H</sub> and NOE data. Double-headed arrows show the observed NOEs in NOESY and (or) ROESY spectra of PRM2, NAPRM2, or PAPRM2. Coupling constants and multiplicities are depicted in parentheses.

carbon chemical shifts between the two toxins were less than 0.1 and 1.0 ppm, respectively, except for those of C78–C82. Second, there were two additional oxymethine-methylene carbon sequences from C1'' to C5'' and from C1''' to C6''' in PRM1 (Table 3). Judging from the difference in molecular weight of 294 mu and the chemical shifts for these spin connectivities, one pentose and one hexose were inferred to be present in the C78–C82 region of the molecule connected by glycosidic bonds to hydroxyl groups. The pseudomolecular ion peak at around *m/z* 2265 was accompanied by ions at *m/z* 2117, 1969, and 1836 in the ESI mass spectra, suggesting that they were generated

(39) A weak NOE was observed between H61 and H62 in the NOESY spectra of both PRM2 and NAPRM2. Although H61 and H62 were *anti*-oriented with each other in the proposed conformer, a minor *gauche* rotamer was presumed, since the 8.5 Hz of <sup>3</sup>J<sub>H61–H62</sub> was slightly deviated from the typical <sup>3</sup>J<sub>H–H</sub> 10–11 Hz for *anti* H/H orientation. The intense NOE observed for H61/H63a in the NOESY of NAPRM2 also supported the presence of a *gauche* rotamer.

Table 3. <sup>1</sup>H and <sup>13</sup>C NMR Assignments of NAPRM1

postm	<sup>13</sup> C <sup>a</sup>	<sup>1</sup> H <sup>b</sup>	postm	<sup>13</sup> C <sup>a</sup>	<sup>1</sup> H <sup>b</sup>	postm	<sup>13</sup> C <sup>a</sup>	<sup>1</sup> H <sup>b</sup>	postm	<sup>13</sup> C <sup>a</sup>	<sup>1</sup> H <sup>b</sup>	postm	<sup>13</sup> C <sup>a</sup>	<sup>1</sup> H <sup>b</sup>
1	131.0	6.54	18	131.8	6.16	32	72.3	4.12	45	81.2	3.24	60	65.7	4.29
2	115.8	5.91	19	133.6	5.53	33	86.6	2.91	46	75.6	3.86	61	84.4	3.17
3	78.0		20	79.1	3.77	34	75.8	3.79	47	36.2	1.60	62	76.6	3.63
4	93.6		21	32.9	1.34	35	32.1	1.36	48	66.3	4.21	63	29.8	1.17
5	21.0	2.40	22	30.6	1.56	36	30.4	2.00	49	82.0	3.00	64	30.4	1.26
6	21.0	2.45			1.40			1.93	50	70.5	3.78	65	77.9	2.88
7	92.6				1.86			3.08	51	41.3	1.64	66	80.9	3.55
8	82.2		23	79.3	2.92	37	77.3	3.09	52	67.5	3.63	67	74.6	3.83
9	111.7	5.52	24	78.4	3.06	38	83.8	3.09	53	85.2	3.48	68	70.8	4.46
10	142.8	6.45	25	37.4	1.49	39	31.1	1.99	54	73.8	4.47	69	77.8	3.90
11	133.8	6.04	26	78.3	2.26	40	38.1	1.41	55	35.3	2.02	70	73.2	4.51
12	134.8	5.69	27	78.3	3.01	41	76.2	3.09	56	60.3	4.46	71	71.0	4.34
13	39.0		28	39.5	1.46	42	80.9	2.78	57	80.3	3.14	72	73.3	4.33
14	50.5	4.04	29	77.5	4.13	43	30.8	1.36	58	69.2	4.27	73	71.2	3.96
15	39.0		30	82.0	3.37	44	28.9	1.35	59	38.4	1.60	74	74.7	4.29
16	132.1	5.62	31	38.7	2.08			1.76				75	37.3	1.95
17	133.9	6.00			2.31									2.24

<sup>a</sup> <sup>13</sup>CD<sub>3</sub>OD was adjusted to 50.0 ppm in CD<sub>3</sub>OD/D<sub>2</sub>O (1:1) at 125 MHz. <sup>b</sup> CD<sub>2</sub>HOD was adjusted to 3.31 ppm in CD<sub>3</sub>OD/C<sub>5</sub>D<sub>5</sub>N (1:1) at 400 MHz. <sup>c</sup> Denotes each assignment is interchangeable. <sup>d</sup> Not observed.

by cleavage of three glycosidic bonds (see Supporting Information). Comparison of both chemical shifts and coupling constants with those in the literature<sup>40</sup> allowed us to deduce that the pentose was an  $\alpha$ -arabino-pyranose and the hexose was a  $\beta$ -pento (-galacto- or -gluco-) furanose. HMBC correlations for H1''/C82 and H1'''/C4''' coupled with strong NOEs for H1''/H78 and H1'''/H82 clearly indicated that the pentose and hexose were linked via C78 OH and C82 OH, respectively. These sugars were determined to be L-arabinose for the pentose and D-galactose for the hexose by GC analyses with a chiral column using the same procedure as for PRM2. The pentofuranose at C77 was initially considered to be L-xylose, as is the case with PRM2, due to the resemblance of the chemical shifts. However, the GC analysis of hydrolysates unexpectedly disclosed that the pentofuranose in PRM1 was not L-xylose but was D-ribose (see Supporting Information). These data allowed us to conclude that PRM1 possessed three different monosaccharide moieties,  $\alpha$ -D-ribofuranose,  $\alpha$ -L-arabinopyranose, and  $\beta$ -D-galactofuranose, at C77, C78, and C82, respectively, on the same aglycone structure of PRM2 (Figure 1). By extensively comparing the chemical shifts, coupling constants, and NOESY data between NAPRM2 and NAPRM1, the relative stereochemistry in the cyclic parts from rings A to N in PRM1 was concluded to be the same as that in PRM2 (see Supporting Information).

The present study has revealed the structures for both prymnesin-1 and prymnesin-2 and their partial configurations. Although 10 chiral centers in the acyclic parts of the aglycone remain unassigned, these results led to the gross structures of the legendary red tide toxins "prymnesins". They possess unique structural features, represented by a single chain of 90 carbons encompassing repeated *trans*-1,6-dioxadecaline units and the conjugated double/triple bonds at both termini. The presence of chlorine and nitrogen atoms is also unusual in polyether compounds. Sugars and hydroxyl groups are unevenly distributed, congesting the western half (C48–C85) of the molecule and giving the molecule an amphiphilic property. These characteristics may play an important role in their extremely potent bioactivities.

As was the case in maitotoxin, the <sup>13</sup>C-enrichment technique was very effective in structural elucidation of prymnesins, which were poorly soluble in NMR solvents and are large and complicated molecules. Preparation of derivatives and measure-

(40) The chemical shifts and some of the coupling constants for three sugar moieties in NAPRM1 are as follows; the pentofuranose C1' ( $\delta$  106.1, 5.28, d,  $J$  = 4 Hz), C2' ( $\delta$  74.1, 4.20), C3' ( $\delta$  72.5, 4.16), C4' ( $\delta$  87.8, 4.41), and C5' ( $\delta$  63.8, 3.64, 3.69, dd,  $J$  = 3, 11 Hz); the pentopyranose C1'' ( $\delta$  106.0, 4.88, d,  $J$  = 6.5 Hz), C2'' ( $\delta$  73.7, 4.03,  $J^*$  = 7, 9 Hz), C3'' ( $\delta$  75.2, 3.73,  $J^*$  = 4, 9 Hz), C4'' ( $\delta$  70.4, 3.89), and C5'' ( $\delta$  64.5, 3.47, 4.04); the hexosofuranose C1''' ( $\delta$  110.4, 5.52, d,  $J$  = 7 Hz), C2''' ( $\delta$  84.3, 4.52), C3''' ( $\delta$  78.5, 4.54), C4''' ( $\delta$  85.1, 4.43), C5''' ( $\delta$  72.7, 4.07), and C6''' ( $\delta$  65.2, 3.94). Based on the literature values cited above (23 b,c), the pentofuranose (C1'–C5') was determined as  $\alpha$ -anomer. Based on the similarity of chemical shifts and/or coupling constants with the following NMR data in the literature, the pentopyranose (C1''–C5'') and the hexofuranose (C1'''–C5''') were deduced to be  $\alpha$ -arabinopyranose and  $\beta$ -galactofuranose, respectively. <sup>13</sup>C data for  $\alpha$ -arabinopyranoside: C1 ( $\delta$  105.1), C2 ( $\delta$  71.8), C3 ( $\delta$  73.4), C4 ( $\delta$  69.4), C5 ( $\delta$  67.3);  $\beta$ -arabinopyranoside: C1 ( $\delta$  101.0), C2 ( $\delta$  69.4), C3 ( $\delta$  69.9), C4 ( $\delta$  70.0), C5 ( $\delta$  63.8);  $\alpha$ -galactofuranoside: C1 ( $\delta$  103.8), C2 ( $\delta$  78.2), C3 ( $\delta$  76.2), C4 ( $\delta$  83.1), C5 ( $\delta$  74.5), C6 ( $\delta$  64.1);  $\beta$ -galactofuranoside: C1 ( $\delta$  109.9), C2 ( $\delta$  81.3), C3 ( $\delta$  78.4), C4 ( $\delta$  84.7), C5 ( $\delta$  71.7), C6 ( $\delta$  63.6);  $\alpha$ -glucofuranoside: C1 ( $\delta$  104.0), C2 ( $\delta$  77.7), C3 ( $\delta$  76.6), C4 ( $\delta$  78.8), C5 ( $\delta$  70.7), C6 ( $\delta$  64.2);  $\beta$ -glucofuranoside: C1 ( $\delta$  110.0), C2 ( $\delta$  80.6), C3 ( $\delta$  75.8), C4 ( $\delta$  82.3), C5 ( $\delta$  70.7), C6 ( $\delta$  64.5) in the literature;<sup>23a</sup> <sup>1</sup>H data for  $\alpha$ -arabinopyranose: H1 ( $\delta$  4.60,  $J_{1,2}$  = 7.2 Hz), H2 ( $\delta$  3.58,  $J_{2,3}$  = 9.9 Hz), H3 ( $\delta$  3.75,  $J_{3,4}$  = 3.6 Hz);  $\beta$ -arabinopyranose: H1 ( $\delta$  5.34,  $J_{1,2}$  = 3.6 Hz), H2 ( $\delta$  3.93,  $J_{2,3}$  = 9.3 Hz), H3 ( $\delta$  3.93,  $J_{3,4}$  = 9.8 Hz); in Lemieux, R. U.; Stevens, J. D. *Can. J. Chem.* **1966**, *44*, 249. (\*The coupling constants were deduced from the cross-peaks in the <sup>1</sup>H–<sup>1</sup>H COSY spectrum of NAPRM1.)

ment in different NMR solvents were also a key to success. From a biosynthetic point of view, prymnesins are the first example of *trans*-fused cyclic polyethers that were produced by a microalga other than dinoflagellates. We believe that the present structural elucidation should contribute to future investigations on the mode of action of their potent ichthyotoxic and hemolytic activities and stimulate biosynthetic studies on phytoflagellate metabolites. Elucidation of the 10 remaining unresolved chiral centers in prymnesins and their absolute stereochemistries should offer new challenges to organic chemists.

## Experimental Section

To conserve space in the article, "chemicals" and "spectral measurement" are described in Supporting Information.

**Culture of *Prymnesium parvum* and Isolation of Prymnesins.** As reported previously, the *P. parvum* strain used in our studies<sup>7,8,41</sup> was a generous gift from Professor L. R. Berger, University of Hawaii which had originated in Israel. The unialgal culture was not axenic. The culture for the toxin production was basically achieved with 4 L of SW-II medium<sup>42</sup> in a 5-L shaking bottle kept at 25 °C with strong aeration (100 mL/sec) for about 2 weeks under an 18 h/6 h light/dark cycle. We obtained the total of 600 L of conventional culture, and another 180 L of culture in the presence of Na<sub>2</sub><sup>13</sup>CO<sub>3</sub> (50 mg/L). Two-thirds of the conventional culture (400 L) was used for the isolation of prymnesins and the rest was consumed both to establish the optimum purification conditions and to prepare synthetic derivatives of prymnesin-2. The purification procedures were basically the same as mentioned previously<sup>8</sup> with the following modifications. Usually, about 60 g of the fresh algal cells of *P. parvum* harvested by continuous flow centrifugation (5 000 G, 100 mL/min) from 60 L cultured media, was recentrifuged at higher speed (10 000 G, 10 min) to eliminate excess water. Thereafter, greenish pigments, e.g., chlorophyll, were removed from the cells by washing with cold acetone 4–5 times. The toxic residue was extracted with MeOH three times and then with aqueous propanol (PrOH/H<sub>2</sub>O 8:2) once with homogenizing. The combined yellowish extract was evaporated to a small volume, suspended in H<sub>2</sub>O, and defatted 3–4 times with ethyl acetate. The toxic aqueous layer was mixed with a quarter volume of PrOH and then loaded on a column of Fuji Gel ODS-Q3 (Wako Pure Chemicals, 20 × 250 mm), which had been washed successively with 1:10 saturated solution of EDTA-2Na and H<sub>2</sub>O. The crude toxins retained on the column were eluted with PrOH/H<sub>2</sub>O (8:2) and then evaporated in a brown flask (brown glassware was used throughout the following procedure). The toxic residue was dissolved in a small amount of PrOH/H<sub>2</sub>O (2:8) and then loaded on a HW-40 column (Toyopearl superfine Tosoh, 10 × 250 mm) which had previously been equilibrated with PrOH/H<sub>2</sub>O (2:8) after conditioning three times with the EDTA-2Na solution. After washing successively with PrOH/H<sub>2</sub>O (2:8) and (1:1), crude toxins were eluted with PrOH/2 mM AcOH (1:1). The toxins were obtained only in the acidic eluate. The crude toxins from the acidic fraction were then desalted on a SEP-PAK C18 cartridge (Waters), which was conditioned previously by consecutively washing with MeOH, PrOH/H<sub>2</sub>O(8:2), H<sub>2</sub>O, the EDTA solution, and PrOH/H<sub>2</sub>O (2:8). The retained toxins were then eluted with PrOH/H<sub>2</sub>O (3:2) and further subjected to final purification by HPLC using Develosil ODS-7 (Nomura Chemicals) with PrOH/2 mM AcOH (1:1). In this chromatography, prymnesin-1 was eluted ahead of prymnesin-2, due to its higher polarity arising from the two additional sugar moieties. The acetic acid in the eluates was partially removed by evaporation and finally by lyophilization. The toxins in the purification procedure were monitored by TLC (Silica gel-60, Merck; CHCl<sub>3</sub>/MeOH/H<sub>2</sub>O, 55:35:8) and HPLC (TSK gel ODS, Tosoh; PrOH-4 mM AcOH, 3:2), in addition to the previously described hemolytic test. From 400 L culture, 10 mg of prymnesin-1 and 15 mg of prymnesin-2 were obtained. <sup>13</sup>C-

enriched culture 180 L was used for preparation of <sup>13</sup>C-enriched specimens of *N*-acetates (1.5 and 1.6 mg).

***N*-Acetylprymnesins.** The crude toxin solution containing approximately 5 mg prymnesins, which was eluted from Toyopearl HW-40 superfine, was concentrated to a small volume and then suspended in 4 mL of PrOH/H<sub>2</sub>O (3:2) in a 5 mL-reaction tube. To the suspension was added 200 μL of acetic anhydride and the suspension was stirred for 12 h at 30 °C. Subsequently, the reaction mixture was purified with a SEP-PAK C18 cartridge in a similar manner as for the prymnesins. For elution PrOH/H<sub>2</sub>O (1:1) was used instead of PrOH/H<sub>2</sub>O (3:2). Next, *N*-acetylprymnesin-1 and -2 were separated on a Cosmosil 5C-18AR column (Nakarai Tesque) with PrOH/H<sub>2</sub>O (1:1), to furnish approximately 2 mg each of *N*-acetylprymnesin-1 and -2 after lyophilization. Likewise 1.5 mg of *N*-acetylprymnesin-1 and 1.6 mg of *N*-acetylprymnesin-2 were prepared from the <sup>13</sup>C enriched cultures.

**Peracetylprymnesin-2.** Prymnesin-2 (approximately 1.5 mg) was dissolved in 500 μL of dry pyridine in a 2 mL-reaction tube and mixed with 500 μL acetic anhydride. After stirring for 48 h at 30 °C, the reaction mixture was evaporated to a small volume and lyophilized. The reaction was monitored by TLC, HPLC (YMC Pack ODS, Yamamura Chemical; acetonitrile/H<sub>2</sub>O, 9:1), and ESI-MS. Chromatographic and spectroscopic data indicated that the reaction was 90% complete after 48 h.

**1-Dechloro-perhydroprymnesin-2.** The HPLC-purified fraction containing approximately 1.5 mg of prymnesin-2 was concentrated and combined with 30 mL of PrOH/50 mM AcOH (4:1). About 10 mg of palladium hydroxide on carbon was washed three times with the same solvent and added to the solution. The solution was stirred for 4 h under 1.5 atm H<sub>2</sub> at 30 °C. Progress was checked by TLC. After the reaction was complete, the mixture was filtered (ADVANTEC No.5A) and the solution was extracted with EtOAc. Condensation of the aqueous layer yielded 1.2 mg of the reaction product. Purity was confirmed by MS and NMR measurements. These spectra showed that a chlorine atom at C1 of prymnesin-2 was replaced with hydrogen during the reaction.

**Elimination of hydrogen chloride from Prymnesin-2 and *N*-acetylprymnesin-2.** One milligram of *N*-acetylprymnesin-2 was dissolved in 0.8 mL of C<sub>5</sub>D<sub>5</sub>N/CD<sub>3</sub>OD (1:1) in an NMR tube and was kept at 50 °C for 7 days. Elimination of chlorine on C85 and H86 was monitored by NMR measurement on days 1, 3, 5, and 7. Finally, completion of the reaction was confirmed by ESI-MS and NMR. About 200 μg of 85-dechloro-86-dehydroprymnesin-2 was also prepared under virtually the same conditions.

**Acknowledgment.** The present study was supported by a grant from the Ministry of Education, Science, Sports, and Culture, Japan (No. 0710202) and the Naito Foundation. We are grateful to Professor M. Murata, Department of Chemistry, Graduate School of Science, Osaka University, for valuable discussions. Thanks are also due to Dr. S. Matsunaga, Faculty of Agriculture, the University of Tokyo, for determining the sugars; to Mr. K. Kushida, Varian Japan Ltd for NMR measurements; to Mr. S. Aritake for culturing *P. parvum*; to Professor L. R. Berger, University of Hawaii, for donation of *P. parvum* strain; to Dr. A. Morohashi for preparing a part of peracetylprymnesin-2; and to Professor P. J. Scheuer, University of Hawaii, for critical reading of the manuscript.

**Supporting Information Available:** Descriptions for chemicals and spectral measurements of Experimental Section. Partial HMBC spectrum of NAPRM2 indicating the split cross-peaks of C1/H1. The <sup>1</sup>H–<sup>1</sup>H COSY spectrum of peracetylprymnesin-2 with the assignments of cross-peaks. Figures of the alternative regio-isomers for rings D–F, F–I, H–K, and J–M, indicating that they are not supported by NMR data. A figure of two possible conformations in rings F–G, demonstrating that the structure disagrees with an observed NOE. Partial NOESY spectrum of **2**, showing the NOE correlations between H60/H61, H59/H61, H63/H61, H55a/H52, H52/H54, H53/H54, and

(41) Igarashi, T.; Oshima, Y.; Murata, M.; Yasumoto, T. *Harmful Marine Algal Blooms*; Lassus, P., Arzul, G., Erard-LeDenn, E., Gentien, P., Marcaillou-LeBaut, C., Eds.; Lavoisier Publishing: 1994; pp 303–308.

(42) Iwasaki, H. *Biol. Bull.* **1961**, *121*, 173–187.

H55a/H54. Positive ion ESI mass spectrum of **1**, showing ion peaks generated by the cleavage of three glycosidic bonds. Chiral GC chromatograms for determination of sugars in prymnesin-1. The NOESY spectrum of NAPRM1 with the

assignments of cross-peaks (PDF). This material is available free of charge via the Internet at <http://pubs.acs.org>.

JA991740E